공학박사 학위논문

Evolution of {100} texture induced by surface nucleation during γ → α phase transformation in electrical steel

전기강판 재료에서 감마 → 알파 상변태를 이용한 표면핵생성 및 {100} 집합조직 형성 연구

2023년 2월

서울대학교 대학원

재료공학부

정 용 권

Evolution of {100} texture induced by surface nucleation during γ → α phase transformation in electrical steel

지도교수 황 농 문

이 논문을 공학박사 학위논문으로 제출함

2023년 2월

서울대학교 대학원
재료공학부

정 용 권

정용권의 박사 학위논문을 인준함
2023년 2월

위 원 장 한 홍 남
부 위 원 장 황 농 문
위 원 박 은 수
위 원 한 찬 희
위 원 권 수 빈

Abstract

Evolution of {100} texture induced by surface nucleation during γ → α phase transformation in electrical steel

Yong-Kwon Jeong

Materials Science and Engineering

The Graduate School

Seoul National University

Previously, it was shown that the {100}<0vw> texture could be evolved when the specimen is under the appropriate stress during γ → α phase transformation. Here the effect of the various process conditions on the evolution of the {100}<0vw> texture was examined. The texture evolution was affected by the magnitude of tensile stress, the furnace atmosphere, the heat treatment time (or grain size) and the cooling rate. In Fe-1wt%Si, the {100}<0vw> texture was 78.3% under the H_2 atmosphere with a flow rate of 1000 standard cubic centimeter per minute (sccm) whereas it was 16.2% under the N_2 atmosphere with a flow rate of 1000 sccm. The

marked decrease in the percentage of the {100}<0vw> texture under the N_2 atmosphere is believed to be related with the surface oxidation of the specimen. In Fe-2wt%Si-1wt%Ni, the {100}<0vw> texture was 8.9% when the specimen was heat treated at 1100 ℃ for 5 min whereas it increased to 66.0% when the specimen was heat treated for 6 h. This increase of the {100}<0vw> texture is believed to be related with the increase in the grain size. Under the optimum processing condition, the {100}<0vw> texture could be increased to as high as 92.6% in Fe-2wt%Si-1wt%Ni.

In order to study the effect of the uniaxial compressive stress on the development of a cube-on-face texture, two sheet samples were heat treated with different positions to have a different self-load, resulting in a different stress. One specimen was heat treated at 1120 ℃ for 60 min with the broad face positioned horizontally to the specimen holder and the other specimen was heat treated with the broad face positioned vertically to the specimen holder with the other condition being the same. The former produced a weak {100}<0vw> texture, being only 30.9% whereas the latter produced a strong {100}<0vw> texture, being 81.1%. We found out that such a texture difference is related to the difference in the nucleation barrier coming from the stress disparity. Based on this understanding, specimens with a different percentage of the {100}<0vw> texture could be manufactured. The measurements of magnetic properties showed that the specimen with 78.4% of {100}<0vw> and 3.2% of {111}<uvw> had B_{50} = 1.75 and $W_{15/50}$ =

2.19, but the specimen with 0.7% of {100}<0vw> and 81.3% of {111}<uvw> had B_{50} = 1.61 and $W_{15/50}$ = 2.50. The results show that the magnetic flux density of B_{50} was increased by 8.7% and the eddy current loss of $W_{15/50}$ was decreased by 12.4% due to the evolution of the {100}<0vw> texture.

Keyword : Electrical steel; Phase transformation; Cube-on-face; {100}; Texture; Electron backscattering diffraction (EBSD)

Student Number : 2017-28846

Table of Contents

Chapter 1. Introduction.....1

1.1. Electrical steel & cube-on-face texture

Chapter 2. Evolution of {100}<0vw> texture induced by tensile stress in Fe-1wt%Si.....5

2.1. Experimental procedure

2.2. Results

2.3. Discussion

Chapter 3. Evolution of {100}<0vw> texture induced by tensile stress in Fe-2wt%Si-1wt%Ni.....22

3.1. Experimental procedure

3.2. Results

3.3. Discussion

Chapter 4. Evolution of {100}<0vw> texture induced by compressive stress in Fe-2wt%Si-1wt%Ni.....41

4.1. Experimental procedure

4.2. Results and discussion

Chapter 5. Conclusions.....59

Bibliography.....60

Abstract in Korean.....63

List of Figures

Figure 2.1. Schematics showing (a) the specimen suspended in the vertical tube furnace and (b) the numbered locations for EBSD analysis with their stress values indicated.

Figure 2.2. EBSD inverse pole figure normal direction (ND) maps of (a) position 1, (b) position 12 and (c) position 19 of Fe-1wt%Si in Fig. 2.1b heated for 5 min at 1100 ℃. (d)-(f) are orientation distribution functions (ODFs) at $\varphi_2 = 45^\circ$ section, respectively, for (a)-(c).

Figure 2.3. EBSD inverse pole figure ND maps of position 1 of Fe-1wt%Si in Fig. 2.1b heated for 5 min at 1100 ℃ under the flowing gas of (a) H_2 100 sccm and (b) N_2 1000 sccm. (c) and (d) are ODFs at $\varphi_2 = 45^\circ$ section, respectively, for (a) and (b).

Figure 2.4. Cross-sectional TEM images of Fe-1wt%Si heated for 5 min at 1100 ℃ under the flowing gas of (a) H_2 1000 sccm, (b) H_2 100 sccm and (c) N_2 1000 sccm.

Figure 3.1. Schematics of the heat treatment in Fe-2wt%Si-1wt%Ni with varying (a) holding time and (b) cooling rate.

Figure 3.2. EBSD inverse pole figure ND maps of position 1 of Fe-2wt%Si-1wt%Ni in Fig. 2.1b heated at 1100 ℃ for (a) 5 min, (b) 3 h and (c) 6 h. (d)-(f) are ODFs at $\varphi_2 = 45^\circ$ section, respectively, for (a)-(c).

Figure 3.3. EBSD inverse pole figure ND maps of position 19 of Fe-2wt%Si-1wt%Ni in Fig. 2.1b heated at 1100 °C for (a) 5 min, (b) 3 h and (c) 6 h. (d)-(f) are ODFs at $\varphi_2 = 45^\circ$ section, respectively, for (a)-(c).

Figure 3.4. EBSD inverse pole figure ND maps of (a) position 1 and (b) position 19 of Fe-2wt%Si-1wt%Ni in Fig. 2.1b cooled at 16.7 ℃/min from 1000 to 900 ℃. (c) and (d) are ODFs at $\varphi_2 = 45^\circ$ section, respectively, for (a) and (b).

Figure 3.5. EBSD inverse pole figure ND maps of (a) position 1 and (b) position 19 of Fe-2wt%Si-1wt%Ni in Fig. 2.1b cooled at 0.1 ℃/min from 1000 to 900 ℃. (c)-(d) are ODFs at $\varphi_2 = 45^\circ$ section,

respectively, for (a) and (b).

Figure 4.1. Schematics showing how specimens were placed during heat treatment. The 80 mm × 40 mm face of the specimens lay (a) horizontally and (b) vertically to the nickel plate.

Figure 4.2. EBSD inverse pole figure ND maps of Fe-2wt%Si-1wt%Ni specimens with the 80 mm × 40 mm face lying horizontally to the nickel plate, which were held at 1120 ℃ in H_2 for (a) 1 min, (b) 15 min, and (c) 60 min. (d), (e) and (f) are ODFs at $\varphi_2 = 45^\circ$ section for (a), (b) and (c), respectively.

Figure 4.3. EBSD inverse pole figure ND maps of Fe-2wt%Si-1wt%Ni specimens with the 80 mm × 40 mm face lying vertically to the nickel plate, which were held at 1120 ℃ in H_2 for (a) 1 min, (b) 15 min, and (c) 60 min. (d), (e) and (f) are ODFs at $\varphi_2 = 45^\circ$ section for (a), (b) and (c), respectively.

Figure 4.4. (a) The average grain size of α varying with the holding time at 1120 ℃ for the specimens with the 80 mm × 40 mm face lying vertically (red circle) and horizontally (black square) to the

nickel plate. (b) Percentages of {100} (red triangle and rhombus) and {111} (blue circle and square) varying with annealing time. Solid and dashed lines represent the specimens with the 80 mm × 40 mm face, respectively, lying vertically and horizontally to the nickel plate.

Figure 4.5. EBSD inverse pole figure ND maps of Fe-2wt%Si-1wt%Ni specimens annealed at 700 ℃ for 60 min in H_2 with the 80 mm × 40 mm face lying (a) horizontally and (b) vertically to the nickel plate. (c) and (d) are ODFs at $\varphi_2 = 45^\circ$ section for (a) and (b), respectively.

Figure 4.6. EBSD inverse pole figure ND maps of Fe-2wt%Si-1wt%Ni specimens for measurement of magnetic properties. (a) 78.4%, (b) 35.6% and (c) 0.7% of {100}. (d), (e) and (f) are ODFs at $\varphi_2 = 45^\circ$ section for (a), (b) and (c), respectively.

List of Tables

Table 2.1. Percentages of {100}<0vw> and {111}<uvw>, the average grain size of all grains and that of {100}<0vw> misorientation in parentheses for each position of Fe-1wt%Si heat treated for 5 min at 1100 ℃.

Table 3.1. Percentages of {100}<0vw> and {111}<uvw>, the average grain size of all grains and that of {100}<0vw> misorientation in parentheses for each position of Fe-2wt%Si-1wt%Ni heated for 5 min, 1 h, 3 h and 6 h at 1100 ℃. (See Fig. 3.1a for the heating cycle)

Table 3.2. Percentages of {100}<0vw> and {111}<uvw>, the average grain size of all grains and that of {100}<0vw> misorientation in parentheses for each position of Fe-2wt%Si-1wt%Ni heated for 6 h at 1100 ℃. (See Fig. 3.1a for the heating cycle)

Table 4.1. Magnetic properties of Fe-2wt%Si-1wt%Ni alloys with a different texture.

Chapter 1. Introduction

1.1. Electrical steel & cube-on-face texture

Electrical steel is divided into two kinds according to applications. One is grain-oriented electrical steel [GO], which is used for fixed applications such as transformers on the power pole. The other is non-oriented electrical steel [NO], which is used for rotating application such as an electric motor for automobile, generator and so on. In terms of energy efficiency, both GO and NO steels have the optimum orientation arrangement. {110}<001> and {100}<0vw>, which are called, respectively, a Goss texture and a cube-on-face texture, are optimal, respectively, for GO and NO steel [1].

The development of the strong Goss texture has been studied extensively [2-8] and well established now with the mass production for applications [9]. In comparison, the development of the cube-on-face texture has been studied only by a few, far from being in the production stage. The reason would be that there is no systematic and economic way to produce it. However, the vehicles run by the gasoline engine are being replaced by the motor-driven vehicles and in the near future all the vehicles will be replaced by motordriven ones. Therefore, the development of the energy

efficient motors becomes increasingly important. Here, the development of the cube-on-face electrical steel plays an important role [10-16].

Tomida et al. [17] made the first report showing the possibility of preparing the {100} texture by vaporizing Mn at the surface and subsequently decarburization process using γ → α phase transformation. However, the process has not been commercialized because it took the long process time and required the high vacuum condition. To overcome such disadvantages, Sung et al. [18] used the continuous cooling heat treatment for the γ → α phase transformation and could produce the {100}<0vw> texture under the oxygen partial pressure low enough to inhibit the surface oxidation of the specimen. And they also reported that anisotropic elastic modulus in Fe could affect evolution of the {100}<0vw> texture. In the direction of minimization of strain energy, {100}<0vw> texture was favored to evolve on surface.

Under the continuous cooling heat treatment for the γ → α phase transformation, Kwon et al. [19] reported that the friction stress caused by difference in thermal expansion between steel and Al_2O_3 plates was an important factor for the evolution of the {100}<0vw> texture in Fe-1wt%Si. Ahn et al. [20] also reported that the tensile stress caused by the self-load during heat treatment could induce the evolution of the {100}<0vw> texture in Fe-2wt%Si-1wt%Ni. However, further studies are necessary to find out the specific

process conditions for the optimal evolution of the {100}<0vw> texture.

In this thesis, the variables such as the magnitude of tensile stress, furnace atmosphere, heat treatment time (or grain size) and cooling rate were examined with respect to the evolution of the {100}<0vw> texture. Under the optimum condition determined from these experiments, the Fe-2wt%Si-1wt%Ni specimen with 92.6% {100}<0vw> texture could be prepared.

In our preliminary experiment, it was shown that when α → γ → α phase transformation occurs under the compressive stress, the grain size remarkably increased and produced the strong {100}<0vw> texture. Since the stress on the specimen is an important factor for the {100}<0vw> texture development, a new method was devised to produce the {100}<0vw> texture. Here, a specimen was heat treated at 1100 ℃ with the broad face vertically positioned to induce the high compressive stress in a uniaxial direction by a self-load. The specimen produced a high percentage of the {100}<0vw> texture. To check if the high percentage of the {100}<0vw> texture should come from the compressive stress or not, another specimen was heat treated with the broad face horizontally positioned. In this case, the specimen produced only a low percentage of the {100}<0vw> texture. The purpose of this thesis is to study how the compressive stress affects the texture evolution of {100}<0vw> in Fe-Si steel and a texture evolution

affects magnetic properties.

Chapter 2. Evolution of {100}<0vw> texture induced by tensile stress in Fe-1wt%Si

2.1. Experimental procedure

Ingot of Fe-1wt%Si, which was prepared using induction melting, was hot rolled to 2.3 mm and cold rolled to 0.35 mm thickness. We measured the temperature of the γ → α phase transformation during cooling using the differential scanning calorimetry (DSC) (TGA/DSC1, Mettler Toledo) and determined Ar_3 and Ar_1 temperatures to be ~975 ℃ and ~952 ℃, respectively, for Fe-1wt%Si.

To study the effect of the magnitude of the tensile stress on the development of the {100}<0vw> texture, we hanged the specimens in the vertical tube furnace during the heat treatment as shown in Fig. 2.1a, where the uniaxial tensile stress was applied to the specimen by self-load. In this way, the applied tensile stress would be different depending on the vertical position of the specimen. The quartz cylindrical tube of 50 mm diameter of the vertical furnace was 1500 mm long with a uniform temperature zone of ~400 mm Since the length of the tube is sufficiently long, the gas flow such as H_2 supplied during the experiment is not expected to affect the temperature in the uniform zone. At the bottom of the specimen, the

tensile stress would be zero and continue to increase with increasing vertical position, reaching the maximum stress of 15,190 Pa at the top of the specimen. To estimate the stress, we divided the weight by the cross-section area of the specimen. The length between each position and the specimen end was measured and used to determine the weight of each position.

The specimen size was 200 mm (height) × 20 mm (width) × 0.35 mm (depth). As shown in Fig. 2.1b, the specimen was equally divided into 20 segments indicated by the numeric numbers in the ascending order. The 400 mm uniform zone of the vertical tube furnace was long enough for the 200 mm long specimen to be in the uniform zone during the heat treatment. The texture development of the segment of position 1, which was at the bottom, and the segments of position 7 ~ position 13 and position 19 was analyzed using the electron back-scattered diffraction (EBSD) (EDAX, Hikari) and TSL OIM Analysis 7 software to determine the grain size and orientations.

During heat treatment of the Fe-1wt%Si specimen, H_2 gas (99.9999%) was supplied at the flow rate of 1000 standard cubic centimeter per minute (sccm). The specimens were heated at 10 ℃/min, held for 5 min at 1100 ℃, cooled down to 950 ℃ for 2 h, which corresponds to the cooling rate of 1.25 ℃/min, and then cooled in the furnace. Additionally, in order to see the effect of the heat treatment atmosphere, some Fe-1wt%Si specimens were heat

treated under H_2 (99.9999%, 100 sccm) and N_2 (99.9999%, 1000 sccm). Dew points of H_2 and N_2, which were measured using a dew point detector (GFTH 200, Greisinger), were −35.5 °C and −34.2 °C, respectively. And the oxide layer formed on the specimen surface was analyzed by Cs corrected monochromated TEM/STEM (Themis Z, Thermo Fisher).

2.2. Results

Figure 2.2a–c show the inverse pole figure (IPF) ND maps of the Fe–1wt%Si specimen heat treated for 5 min at 1100 ℃, respectively, for the position 1, 12, and 19 of Fig. 2.1b. Figure 2.2d–f show the corresponding orientation distribution function (ODF) maps sectioned at φ_2 = 45°. Based on the brandon criteria of {hkl} ± 15°, percentages of {100}<0vw> of Fig. 2.2a–c were, respectively, 78.3, 29.2 and 15.0% and those of {111}<uvw> were, respectively, 3.6, 17.8 and 26.3%. Average gran sizes of Fig. 2.2a–c were 242, 190 and 192 μm, respectively. And the data for the other areas were summarized in Table 2.1. As the position of the specimen changes from the bottom to the top, percentages of {100}<0vw> decreased and percentages of {111}<uvw> increased.

On the other hand, Sung et al. [18] reported that the oxygen partial pressure, which would affect the oxidation of the specimen surface, was important in the evolution of the {100}<0vw> texture. Considering this, we studied the effect of the atmospheric condition, which was expected to affect the surface oxidation, on the {100}<0vw> texture evolution in Fe–1wt%Si. Figure 2.3a and b show IPF ND maps of the specimen heat treated under H_2 100 sccm (99.9999%) and N_2 1000 sccm (99.9999%), respectively for the position 1. Figure 2.3c and d show the corresponding ODF maps

sectioned at $\varphi_2 = 45^\circ$. Percentages of {100}<0vw> in Fig. 2.3a and b were, respectively, 20.9 and 16.2% and those of {111}<uvw> were, respectively, 16.6 and 42.3%. The average grain sizes of Fig. 2.3a and b were 263 and 111 μm, respectively.

To observe the thickness of the oxide layer on the specimen surface, cross sections of the specimens of Fig. 2.3a and b were observed by TEM. For comparison, the cross section of the specimen of Fig. 2.2a, which was heat treated under H_2 1000 sccm (99.9999%), was also observed by TEM. In order to distinguish and protect the oxide layer, the specimen surface was coated by Pt followed by carbon coating. The cross section was prepared by focused ion beam (FIB) (SMI3050SE, SII Nanotechnology) before TEM observation. Figure 2.4a–c show the cross sectional TEM images of the specimens for Figs. 2.2a and 2.3a, b, respectively. The white areas in the lower part of Fig. 2.4a–c are the specimen and the black areas in the upper part are carbon. The spherical black areas inside the white area in Fig. 2.4b and c are due to the unwanted contamination during the FIB process. It should be noted that unwanted contamination did not come from the specimen nor from heat treatment but come during the specimen preparation for TEM observation, more specifically, from gallium ion source during the FIB etching. The narrow whitish strip in the boundary between the white and black areas is Pt. The thin regions between the whitish strip and the white area are the oxide layer. The EDS

mapping of this layer consisted of Si and O, implying that the layer should be the silicon oxide. The source of Si would be from Fe-1wt%Si.

The oxide layer of Fig. 2.4a is as thick as 17-27 nm, which might have formed after the specimen was taken out of the furnace at room temperature. The thickness of the oxide layer of Fig. 2.4b is not uniform. In certain areas, it is as thick as ~35 nm but in other area, it was as thick as ~229 nm. On the other hand, the thickness of the oxide layer of Fig. 2.4c is relatively uniform as ~113 nm. Figure 2.4a-c are for the specimens of Figs. 2.2a and 2.3a, b which have, respectively, 78.3, 20.9 and 16.2% of the {100}<0vw> texture. It should be noted that the specimens of Fig. 2.4a-c were taken from the position 1 of Fig. 2.1b. Therefore, they are under the same condition of tensile stress and differ only in the state of the surface oxidation.

2.3. Discussion

2.3.1. Effect of Tensile Stress on the Evolution of the {100}<0vw> Texture

Since the temperature would be uniform along the specimen in Fig. 2.2 the positions of 1, 12 and 19 (See Fig. 2.1b) are expected to differ only in the tensile stress. Therefore, Fig. 2.2, where percentages of {100}<0vw> were 78.3, 29.2% and 15.0%, respectively, at the specimen positions of 1, 12 and 19, indicates that the increase of tensile stress inhibits the evolution of the {100}<0vw> texture. The tensile stress would affect the nucleation barrier. Since the molar volume of α with the body centered cubic (bcc) lattice is larger than γ with the face centered cubic (fcc) lattice, the α nucleus would be under the compressive stress when α nucleates from γ. The nucleation barrier considering the strain energy during the solid-state nucleation is expressed as Eq. (1).

$$\Delta G^* = \frac{16\pi\sigma^3}{3\left(-\Delta f_v + \Delta f_s\right)^{2,}} \qquad (1)$$

where σ is the α/γ interfacial energy, Δf_v is the volume free energy difference between α and γ, and Δf_s is the strain energy. For

elastically isotropic materials, Δf_s is expressed as Eq. (2).

$$\Delta f_s = 4G\delta^2 V, \qquad (2)$$

where G is a shear modulus, δ is a lattice misfit and V is the volume. Since the shear modulus G is proportional to the Young's modulus E, the strain energy Δf_s would be proportional to E.

When the tensile stress is applied by self-load as shown in Fig. 2.1a, it would decrease the compressive stress during the nucleation of α from ɣ, thereby decrease the nucleation barrier and increase the nucleation rate. This aspect is revealed in Fig. 2.2, where average gran sizes were 242, 190 and 192 μm at the positions of 1, 12 and 19, respectively. The small grain size indicates the higher nucleation rate, which again indicates the low nucleation barrier.

Then, why is the percentage of the {100}<0vw> texture affected by the tensile stress or the position of the specimen? In relation to this, it was reported that the Young's modulus E is minimum indirections in Fe [18]. Therefore, the α nucleus with {100}<0vw> would have a minimum nucleation barrier if the nucleation takes place on the surface, as previously suggested by Lee et al. [21] and Sung et al. [18]. This means that if nucleation of α is made to occur exclusively on the surface and these nuclei are made to grow to the entire specimen, the strong {100}<0vw> texture would be evolved.

The problem is that nucleation of α can occur not only on the surface but also in the bulk. In the polycrystalline bulk, the nucleation barrier decreases in the order of grain boundaries, triple junction lines and four grain corners [22]. Although the nucleation barrier at the triple junctions on the surface would be small, it may be comparable to the nucleation barrier at four grain corners in the bulk. Since the number of four grain corners decreases with increasing grain size, the large grain size would make the surface nucleation dominant, which would favor the evolution of the {100}<0vw> texture.

If the tensile stress, which would decrease the compressive stress of Δf_s in Eq. (2) and thereby decrease the nucleation barrier, induce the nucleation at the four grain corners in the bulk, the nuclei would not have the misorientation of {100}<0vw>. Therefore, the tensile stress would have an adverse effect on the evolution of the {100}<0vw> texture. This analysis can explain the largest percentage of the {100}<0vw> texture of Fig. 2.2a, which is taken at the position 1 with the lowest tensile stress.

Considering the high percentage (78.3%) of the {100}<0vw> texture in Fig. 2.2a, the small tensile stress has a beneficial effect on the evolution of the {100}<0vw> texture in comparison with the normal specimen without any stress. In relation to this result, Kwon et al. [19] reported that the small tensile shear stress is favorable for the development of the {100}<0vw> texture during the γ → α

phase transformation in Fe-1wt%Si. They observed that 76.0% of the {100}<0vw> texture was developed in the Fe-1wt%Si specimen placed between alumina plates during cooling from 1100 ℃. They attributed the evolution of the strong {100}<0vw> texture to the frictional stress coming from the difference in the thermal expansion coefficient between the specimen and the alumina plate. The frictional stress would induce the small tensile shear stress. If stress wasn't applied on the specimen, the percentage of {100}<0vw> was only 11.6%. They suggested that the small tensile shear stress decreased the nucleation barrier on the surface, favoring the nucleation of grains with {100}<0vw> misorientations on the surface.

2.3.2. Effect of Heat Treatment Atmosphere on the Evolution of the {100}<0vw> Texture

Comparing the oxidation layers shown in Fig. 2.4 for the specimens of Fig. 2.2a and 2.3a, b with their percentages of the {100}<0vw> texture, we can say that the oxidation layer had an adverse effect on the evolution of the {100}<0vw> texture, which was also reported by Sung et al. [18]. According to the analysis in sect. 2.3.1, the nucleus of α with {100}<0vw> misorientations on the surface contributes to the evolution of the {100}<0vw> texture. The surface oxidation layer would make it difficult for α with

{100}<0vw> misorientations to nucleate on the surface. The experimental fact is that the specimen heated under 1000 sccm H_2 has 78.3% {100}<0vw> and that under 100 sccm H_2 has 20.9% {100}<0vw>. TEM observation of the cross section of the two specimens shows that the specimens heated under 1000 and 100 sccm H_2 have, respectively, oxide layers of 17–27 nm and 35–229 nm. From these results, we think that the surface oxidation layer was completely removed by reduction for the specimen heated under 1000 sccm H_2 during heat treatment and an oxidation layer of 17–27 nm must have been formed after the specimen was taken out from the furnace. In the case of the specimen heated under 100 sccm H_2, however, the oxidation layer was only partly removed and the removal rate was non-uniform, considering the non-uniform thickness of 35–229 nm. The complete and partial removal of the oxide layer, respectively, under 1000 and 100 sccm H_2 would come from the difference in the driving force for reduction. The dew point, which is determined by the partial pressure of H_2O and H_2, would be different between 1000 and 100 sccm H_2 [23]. The rate of non-uniform removal under 100 sccm H_2 might be related to some uncertain kinetic factors, which are difficult to identify. The grain size of Fig. 2.3a is larger than those of Figs. 2.2a and 2.3b. The processing parameter that might be responsible for the difference in the grain size would be the difference in the flow rate of gas. It should be noted that the flow rate of 100 sccm H_2 is 10 times as low as those of Figs. 2.2a and 2.3b. Since an appreciable amount of

heat would be consumed to heat the gas at room temperature to the temperature of the hot zone, the high flow rate could decrease the actual temperature of the heat-treated specimen. Therefore, one possibility for the large grain size in Fig. 2.3a would be that the actual temperature of the specimen of Fig. 2.3a would be higher than those of Figs. 2.2a and 2.3b during heat treatment.

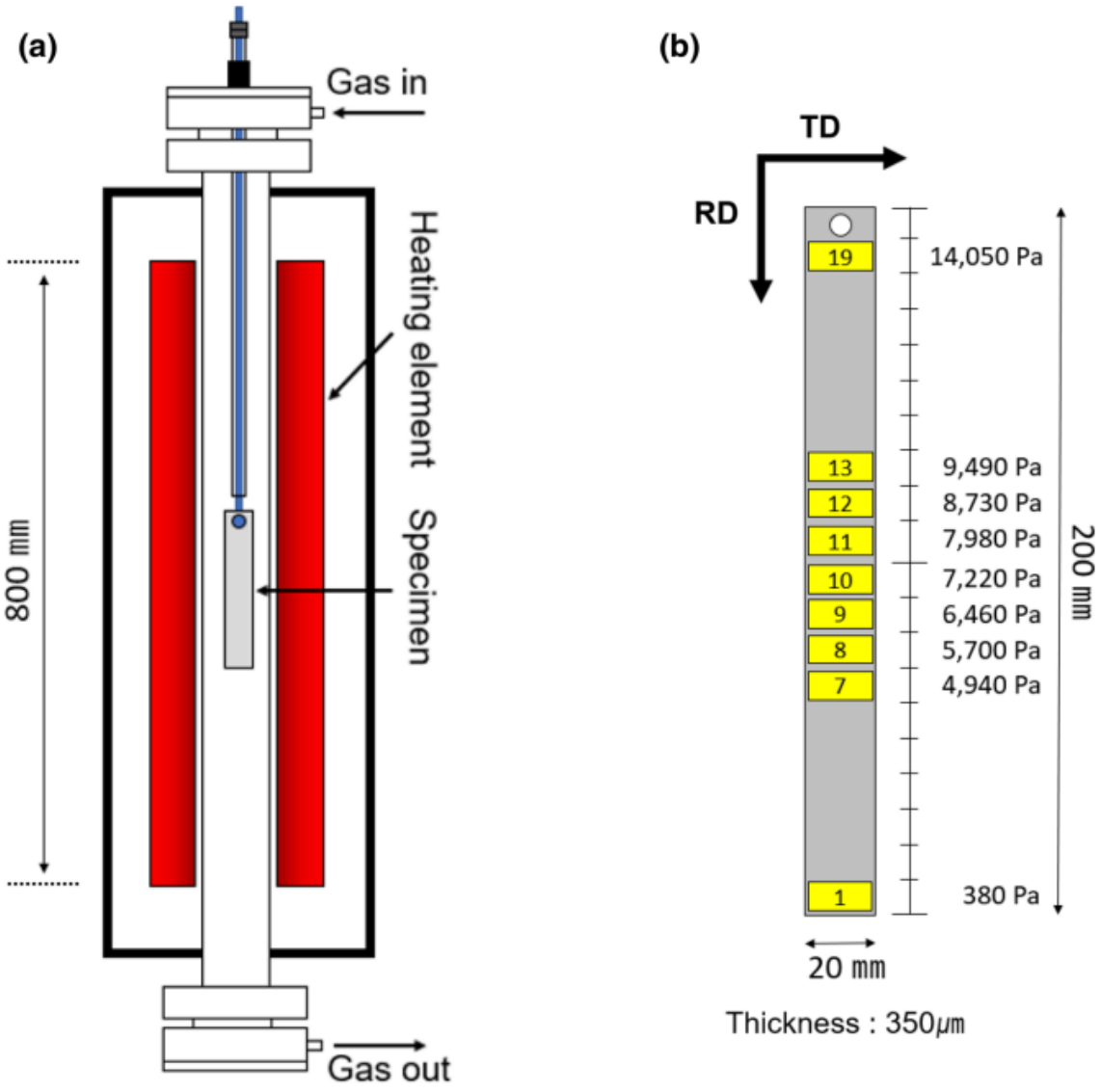

Figure 2.1. Schematics showing (a) the specimen suspended in the vertical tube furnace and (b) the numbered locations for EBSD analysis with their stress values indicated.

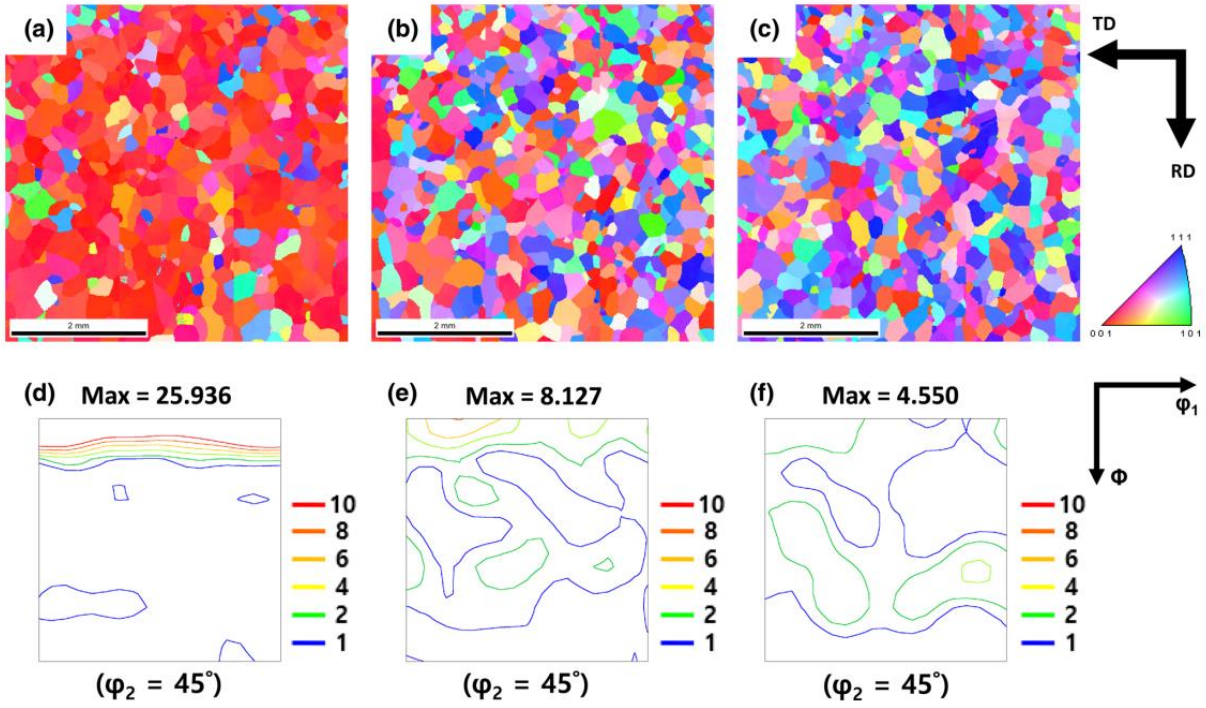

Figure 2.2. EBSD inverse pole figure normal direction (ND) maps of (a) position 1, (b) position 12 and (c) position 19 of Fe-1wt%Si in Fig. 2.1b heated for 5 min at 1100 ℃. (d)-(f) are orientation distribution functions (ODFs) at φ_2 = 45° section, respectively, for (a)-(c).

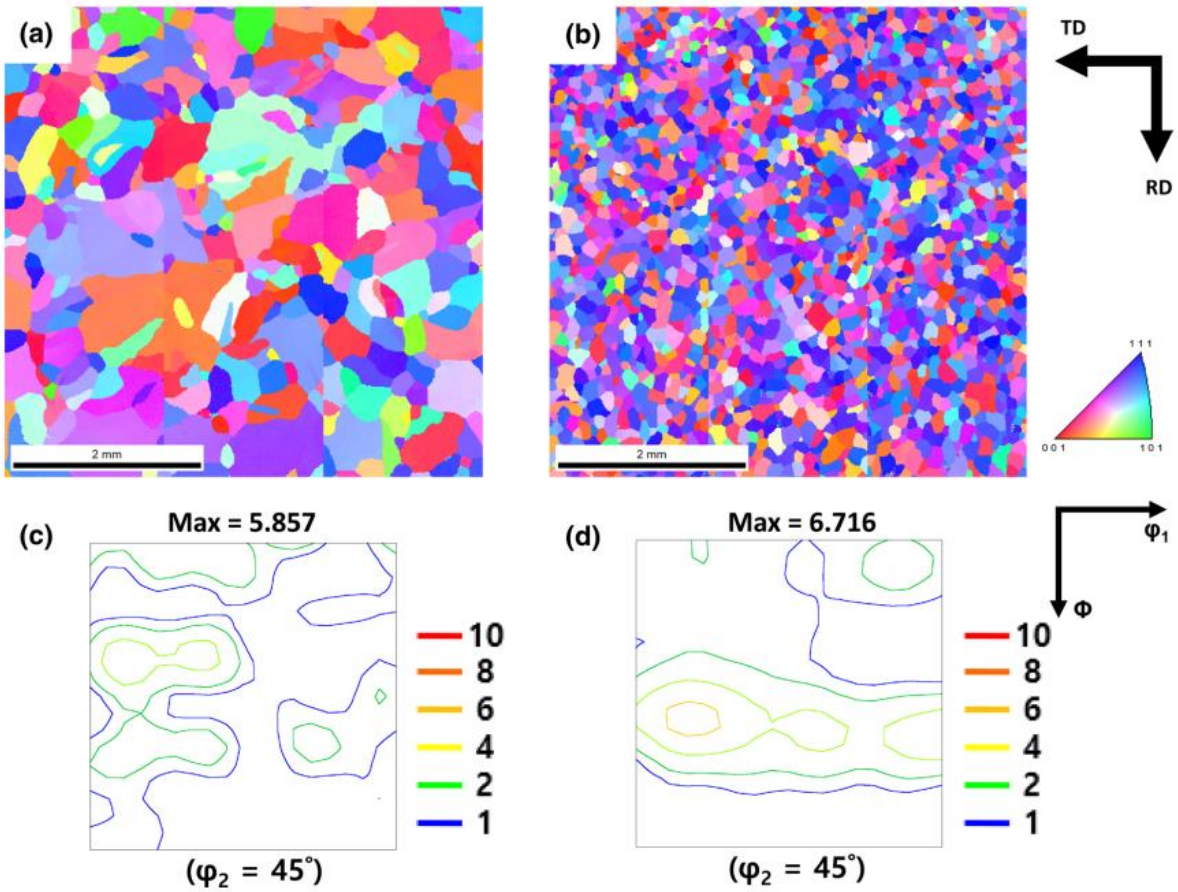

Figure 2.3. EBSD inverse pole figure ND maps of position 1 of Fe-1wt%Si in Fig. 2.1b heated for 5 min at 1100 ℃ under the flowing gas of (a) H_2 100 sccm and (b) N_2 1000 sccm. (c) and (d) are ODFs at $\varphi_2 = 45^\circ$ section, respectively, for (a) and (b).

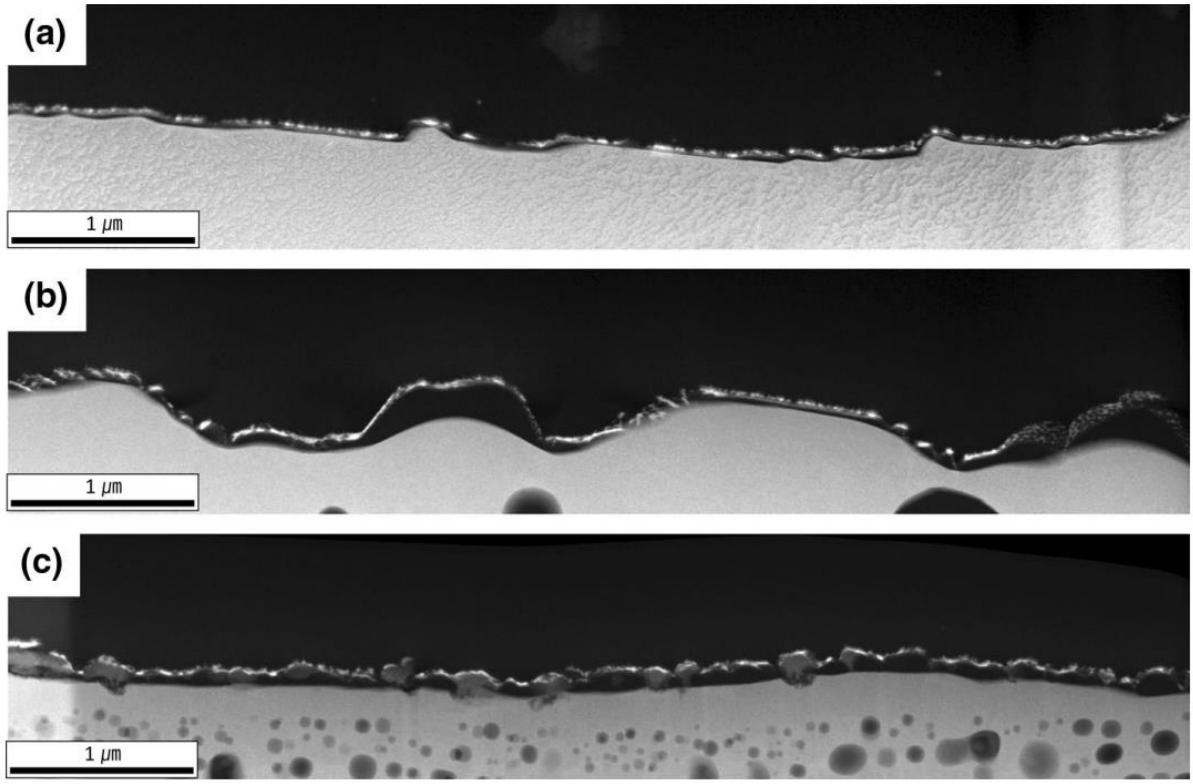

Figure 2.4. Cross-sectional TEM images of Fe-1wt%Si heated for 5 min at 1100 ℃ under the flowing gas of (a) H_2 1000 sccm, (b) H_2 100 sccm and (c) N_2 1000 sccm.

Position of analysis	{100}±15°, (%)	{111}±15°, (%)	Grain size, (μm)
Position 19	15.0	26.3	192 (181)
Position 13	17.0	25.1	197 (191)
Position 12	29.2	17.8	190 (206)
Position 11	60.6	7.6	216 (244)
Position 10	67.6	4.9	217 (242)
Position 9	69.9	6.5	219 (249)
Position 8	72.8	6.1	230 (262)
Position 7	73.6	4.9	230 (256)
Position 1	78.3	3.6	242 (272)

Table 2.1. Percentages of {100}<0vw> and {111}<uvw>, the average grain size of all grains and that of {100}<0vw> misorientation in parentheses for each position of Fe-1wt%Si heat treated for 5 min at 1100 ℃.

Chapter 3. Evolution of {100}<0vw> texture induced by tensile stress in Fe-2wt%Si-1wt%Ni

3.1. Experimental procedure

Ingot of Fe-2wt%Si-1wt%Ni, which was prepared using induction melting, was hot rolled to 2.3 mm and cold rolled to 0.35 mm thickness. In the Fe-Si binary phase diagram, the composition limit of Si for the single γ phase region is about 1.6wt% at 1100 ℃. The two phase (α + γ) region is approximately in the composition range of 1.6-1.85wt%Si at 1100 ℃. This means that if we use an Fe-2wt%Si specimen, the composition should be in the single α phase region at 1100 ℃. This is why we added 1wt%Ni to the 2wt%Si specimen, which made the specimen be in the single γ phase region at 1100 ℃. We measured the temperature of the γ → α phase transformation during cooling using the differential scanning calorimetry (DSC) (TGA/DSC1, Mettler Toledo) and determined Ar_3 and Ar_1 temperatures to be ~955 ℃ and ~928 ℃, respectively, for Fe-2wt%Si-1wt%Ni.

The Fe-2wt%Si-1wt%Ni specimens were heat treated under the same conditions as those of Fe-1wt%Si except that the holding time

in the γ region at 1100 ℃ was varied as 5 min, 1, 3, 6 h under H_2 (99.9999%) at the flow rate of 1000 sccm. Additionally, to study the effect of the cooling rate during γ → α phase transformation on the texture evolution, some specimens were cooled under two additional conditions: being cooled at rates of 16.7 and 0.1 ℃/min during cooling from 1000 to 900 ℃/min after the specimens were held for 6 h at 1100 ℃ and cooled at 1.25 ℃/min from 1100 to 1000 ℃. Schematics of the heat treatment were represented in Fig. 3.1.

3.2. Results

Since the core loss of the electrical steel is decreased with increasing Si content, the effect of the tensile stress on the {100}<0vw> texture was studied also in Fe-2wt%Si-1wt%Ni. Figure 3.2a-c show the IPF ND maps of the position 1 (See Fig. 2.1b) for the Fe-2wt%Si-1wt%Ni specimen heat treated for 5 min, 3 and 6 h at 1100 ℃ (See Fig. 3.1a). Figure 3.2d-f show the corresponding ODF maps sectioned at φ_2 = 45°. Percentages of {100}<0vw> of Fig. 3.2a-c were, respectively, 8.9, 27.5, and 66.0% and those of {111}<uvw> were, respectively, 55.5, 27.8 and 7.3%. Average gran sizes of Fig. 3.2a-c were 117, 222 and 262 μm, respectively.

The result of the position 19 (See Fig. 2.1b) for the Fe-2wt%Si-1wt%Ni specimen is shown in Fig. 3.3. Figure 3.3a-c show the IPF ND maps and Fig. 3.3d-f show the corresponding ODF maps sectioned at φ_2 = 45°. Percentages of {100}<0vw> of Fig. 3.3a-c were, respectively, 10.7, 15.3 and 18.0% and those of {111}<uvw> were, respectively, 59.2, 38.6 and 28.4%. Average gran sizes of Fig. 3.3a-c were, respectively, 109, 212 and 246 μm. And the data of the other areas are summarized in Table 3.1 and 3.2.

The effect of the cooling rate during γ → α transformation on the evolution of the {100}<0vw> texture was studied in Fe-2wt%Si-

1wt%Ni. In the previous experiments for Figs. 3.2 and 3.3, the specimen was cooled from 1100 to 950 ℃ at 1.25 ℃/min and then cooled in the furnace (See Fig. 3.1a). Considering the Ar_3 and Ar_1 temperatures of Fe-2wt%Si-1wt%Ni analyzed by differential scanning calorimetry (DSC) and the ferrite peak of α-{002} during cooling analyzed by in-situ XRD [24], the two phase (α + γ) region is estimated to be in the temperature range of 1000-900 ℃ for the given composition. In the new cooling condition, the Fe-2wt%Si-1wt%Ni specimens were cooled from 1100 to 1000 ℃ at 1.25 ℃/min. Then the specimens were divided into two: one is cooled in the furnace, which would produce the cooling rate of 16.7 ℃/min from 1000 to 900 ℃, and the other is cooled from 1000 to 900 ℃ at 0.1 ℃/min and then cooled in the furnace (See Fig. 3.1b).

Figure 3.4 is for the specimens cooled at 16.7 ℃/min from 1000 to 900 ℃, which corresponds to the highest cooling rate during γ → α transformation. Figure 3.4a and b show, respectively, IPF ND maps of the positions 1 and 19 (See Fig. 2.1b). Figure 3.4c and d show the corresponding ODF maps sectioned at φ_2 = 45°. Percentages of {100}<0vw> in Fig. 3.4a and b were, respectively, 92.6 and 66.3% and those of {111}<uvw> were, respectively, 1.5 and 12.6%. The average grain sizes of all grains and {100}<0vw> misorientation in Fig. 3.4a were, respectively, 327 and 349 μm. The average grain sizes of all grains and {100}<0vw> misorientation in Fig. 3.4b were, respectively, 348 and 427 μm.

Figure 3.5 is for the specimen cooled from 1000 to 900 ℃ at 0.1 ℃ /min and then cooled in the furnace, which corresponds to the slowest cooling rate during γ → α transformation. Figure 3.5a and b show IPF ND maps of the positions 1 and 19 (See Fig. 2.1b). Figure 3.5c and d show the corresponding ODF maps sectioned at φ_2 = 45°. Percentages of {100}<0vw> in Fig. 3.5a and b were, respectively, 48.8 and 20.2% and those of {111}<uvw> were, respectively, 24.8 and 32.4%. The average grain sizes of all grains and {100}<0vw> misorientation in Fig. 3.5a were, respectively, 278 and 286 μm. The average grain sizes of all grains and {100}<0vw> misorientation in Fig. 3.5b were, respectively, 257 and 245 μm.

3.3. Discussion

3.3.1. Effect of Grain Size on the Evolution of the {100}<0vw> Texture in Fe-2wt%Si-1wt%Ni

Under the same heat treatment condition, the percentage of the {100}<0vw> texture changed drastically between Fe-1wt%Si and Fe-2wt%Si-1wt%Ni. The possible reason would be the difference in the grain size, which is 242 μm in Fig. 2.2a and 117 μm in Fig. 3.2a. The reason why the grain size of Fe-2wt%Si-1wt%Ni is much smaller than that of Fe-1wt%Si would come from the solute drag effect of additional Ni and Si of the former. As analyzed in Sect. 2.3.1, the small grain size would increase the number of four grain corners and thereby increase the nuclei without {100}<0vw> misorientations, which would have an adverse effect on the evolution of the {100}<0vw> texture.

If this analysis is correct, the increase in the grain size of the Fe-2wt%Si-1wt%Ni specimens would increase the percentage of the {100}<0vw> texture [20]. The grain size can be increased simply by increasing the heat treatment time. In agreement with this analysis, Fig. 3.2a-c show that the percentages of the {100}<0vw> texture were 8.9, 27.5 and 66.0%, respectively, for the grain sizes of 117, 222 and 262 μm at the position 1.

In Fig. 3.3 for the position 19 (See Fig. 2.1b), however, there was no correlation between the grain size and the percentages of {100}<0vw> texture. In this case, the overall percentage of the {100}<0vw> texture is below 20.0%, which is attributed to the high tensile stress. It appears that the above analysis does not apply to the case under the high tensile stress.

The surface nucleation of {100}<0vw> depends not only on the grain size but also on the tensile stress. Considering the grain size alone, the percentage of the {100}<0vw> texture would be similar between the positions 12 and 19 in Fig. 2.2 (See Fig. 2.1b). Considering the tensile stress, however, the position 19 has higher tensile stress than the position 12 in Fig. 2.2. Therefore, 29.2% of the {100}<0vw> texture at the position 12, which is higher than 15.0% at the position 19, would be attributed to the lower tensile stress at the position 12 in Fig. 2.2.

On the other hand, the grain size of the {100}<0vw> misorientation would increase with its decreasing nucleation rate on the surface. And the nucleation rate on the surface would increase with increasing tensile stress. Therefore, the grain size of the {100}<0vw> misorientation would increase with decreasing position number in Fig. 2.1b of the specimen. This expectation agrees with the grain size of the {100}<0vw> misorientation measured at each position number of the specimen shown in the parenthesis in Table 2.1.

3.3.2. Effect of the Cooling Rate During γ → α Transformation on the Evolution of the {100}<0vw> Texture

Among the three cooling conditions chosen for the specimens of Fig. 3.2c (or Fig. 3.3c), Figs. 3.4 and 3.5, the cooling rate at 16.7 ℃/min from 1000 to 900 ℃ produced the highest percentage, 92.6%, of the {100}<0vw> texture for the position 1. The lowest cooling rate at 0.1 ℃/min from 1000 to 900 ℃ produced the lowest percentage of 48.8% for the position 1 (See Fig. 2.1b). Then, how does the cooling rate affect the evolution of the {100}<0vw> texture? As mentioned earlier, the two phase (α + γ) region is estimated to be in the temperature range of 1000–900 ℃ for Fe–2wt%Si–1wt%Ni.

At the high cooling rate of 16.7 ℃/min, the specimen could not finish the transformation from γ to α in the two phase (α + γ) region at all and the untransformed γ would fall into the single α phase region. Then, the untransformed γ would undergo massive transformation to α. If pre-existing nuclei are mainly formed on the surface and thereby have mainly {100}<0vw> misorientations, they would grow fast to an entire specimen by massive transformation [25]. Then, the high percentage of the {100}<0vw> texture would be evolved.

At the lowest cooling rate of 0.1 ℃/min, however, the specimen stayed roughly for 1000 min in the two phase (α + γ) region, where

the transformation would occur very slowly by the long range diffusion. Even if pre-exiting nuclei with {100}<0vw> misorientations are mainly formed on the surface, they grow only slowly by the long range diffusion in the two phase (α + γ) region. During this period, additional nucleation would occur at low nucleation barriers such as four grain corners in the bulk. If so, the percentage of the {100}<0vw> texture would decrease and the average grain size would decrease because nucleation takes place inside the bulk. This analysis would explain the lowest percentage, 48.8%, of the {100}<0vw> texture in Fig. 3.5a. It would also explain that the grain size in Fig. 3.5a is smaller than that in Fig. 3.4a although the cooling time is much longer in Fig. 3.5a than in Fig. 3.4a.

It should be noted that the cooling rate of 16.7 ℃/min produce a relatively high percentage of 66.3% of the {100}<0vw> texture even at the position 19 (See Fig. 2.1b), which is under the high tensile stress and turns out to be an adverse condition for the evolution of the {100}<0vw> texture in this study. Comparing Fig. 3.2c (or Fig. 3.3c), Figs. 3.4 and 3.5, the cooling rate in the two phase (α + γ) region is very important in inducing the {100}<0vw> texture. The high cooling rate of 16.7 ℃/min in combination with the small tensile stress could produce the {100}<0vw> texture as high as 92.6%. To our knowledge, 92.6% would be the highest percentage of the {100}<0vw> texture reported so far in Fe-2wt%Si.

The average grain sizes of Figs. 3.4b and 3.5a, b are, respectively, 348, 278 and 257 μm. Then, why is the grain size of the specimen in Fig. 3.4b, which was cooled rapidly at 16.7 ℃/min, much larger than those of the specimens in Fig. 3.5a and b, which were cooled slowly at 0.1 ℃/min? Normally, the specimen cooled more slowly has a grain size larger than that cooled rapidly.

To explain the larger grain size of the rapidly cooled specimen in Fig. 3.4b than that of slowly cooled one in Fig. 3.5b, we need to assume that the nucleation rate should decrease with increasing cooling rate. The driving force for the transformation from γ to α starts to form when the temperature of the specimen falls into the two phase (α + γ) region and continues to increase as the temperature decreases. In the two phase (α + γ) region, where the equilibrium composition of the parent γ phase and the newly produced α phase is different, the driving force for the transformation from γ to α is used by long range diffusion. During cooling in the two phase (α + γ) region, the driving force exists for both nucleation and growth of α. Therefore, nucleation can occur at the site of a low nucleation barrier such as four grain corners and three grain edges. During cooling in the two phase (α+ γ) region, lots of nuclei would be formed at four grain corners or three grain edges.

Since the transformation from γ to α by long range diffusion is so slow that the transformation would not complete during cooling in

the two phase (α + γ) region even at 0.1 ℃/min. An appreciable amount of the parent γ phase would remain untransformed even when the temperature of the specimen falls into the single α phase region. In the single α phase region, the composition of the parent γ becomes the same as that of the newly produced α and then the untransformed γ would be transformed to α by massive transformation. However, the grain size would be relatively small because of a large number of nuclei formed in the two phase (α + γ) region during a long residence time.

When the specimen is cooled rapidly at 16.7 ℃/min, however, the specimen resides in the two phase (α + γ) region for a relatively short time before it falls into the single α phase region. The residence time in the two phase (α + γ) region is short, the number of α nuclei would be relatively small. When the specimen falls into the single α phase region, most γ would be untransformed and a relatively small number of α nuclei would grow rapidly by massive transformation. As a result, a relatively large grain size would be produced. This explanation can also be applied to the grain size (327 μm) of the rapidly cooled specimen (16.7 ℃/min) in Fig. 3.4a, which is larger than that (278 μm) of the slowly cooled specimen (0.1 ℃/min) in Fig. 3.5a.

As to the reason why the percentage of the {100}<0vw> misorientation in the rapidly cooled specimen in Fig. 3.4b is as high as 66.3%, which is much higher than 20.2% in the slowly cooled

specimen in Fig. 3.5b, the relative percentage of the nuclei of the {100}<0vw> misorientation on the surface is larger than that of the nuclei of non-cube misorientations at four grain corners or three grain edges in the bulk.

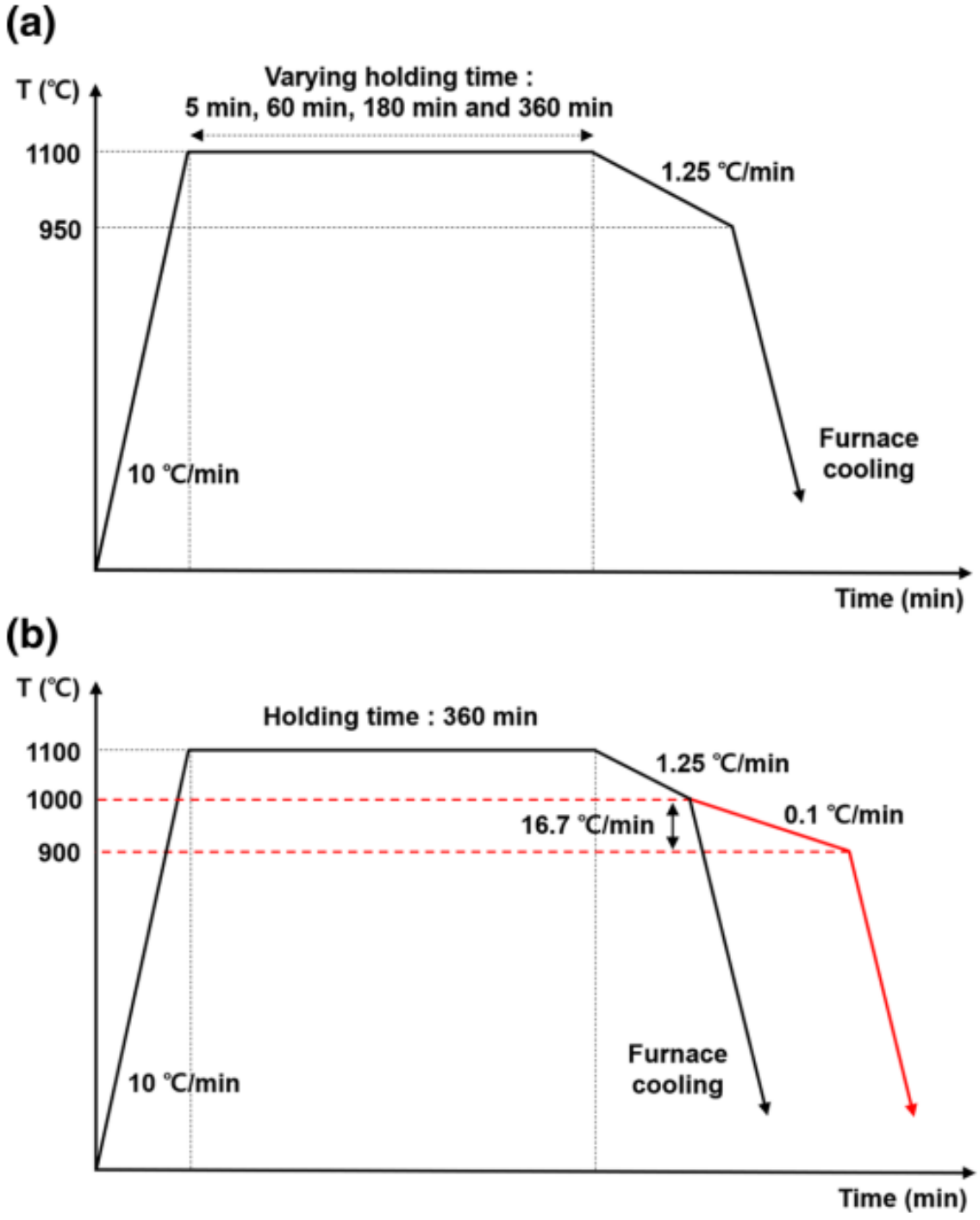

Figure 3.1. Schematics of the heat treatment in Fe-2wt%Si-1wt%Ni with varying (a) holding time and (b) cooling rate.

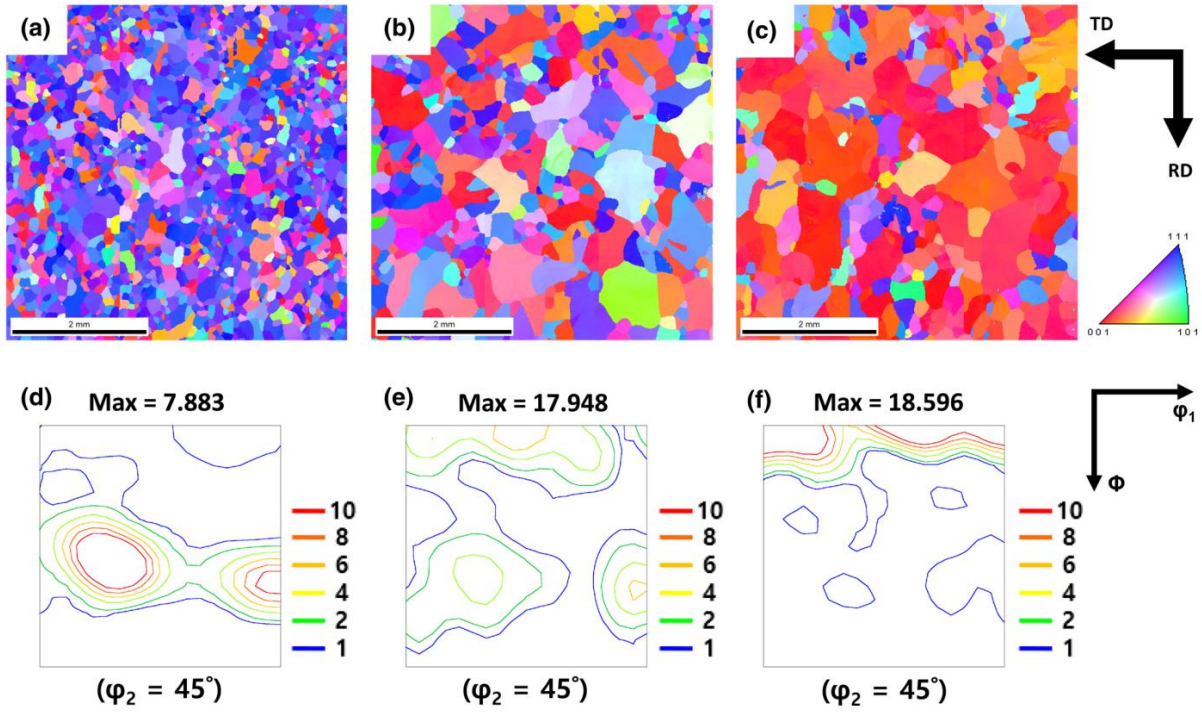

Figure 3.2. EBSD inverse pole figure ND maps of position 1 of Fe–2wt%Si–1wt%Ni in Fig. 2.1b heated at 1100 ℃ for (a) 5 min, (b) 3 h and (c) 6 h. (d)–(f) are ODFs at φ_2 = 45° section, respectively, for (a)–(c).

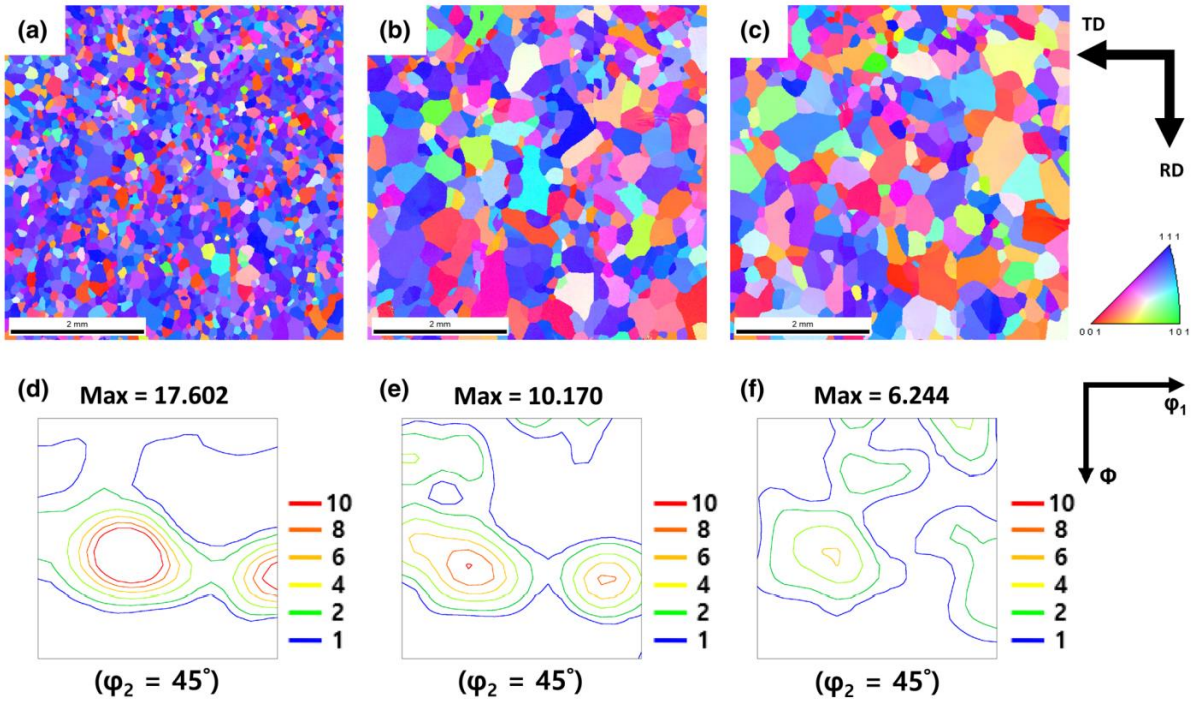

Figure 3.3. EBSD inverse pole figure ND maps of position 19 of Fe–2wt%Si–1wt%Ni in Fig. 2.1b heated at 1100 °C for (a) 5 min, (b) 3 h and (c) 6 h. (d)–(f) are ODFs at $\varphi_2 = 45^\circ$ section, respectively, for (a)–(c).

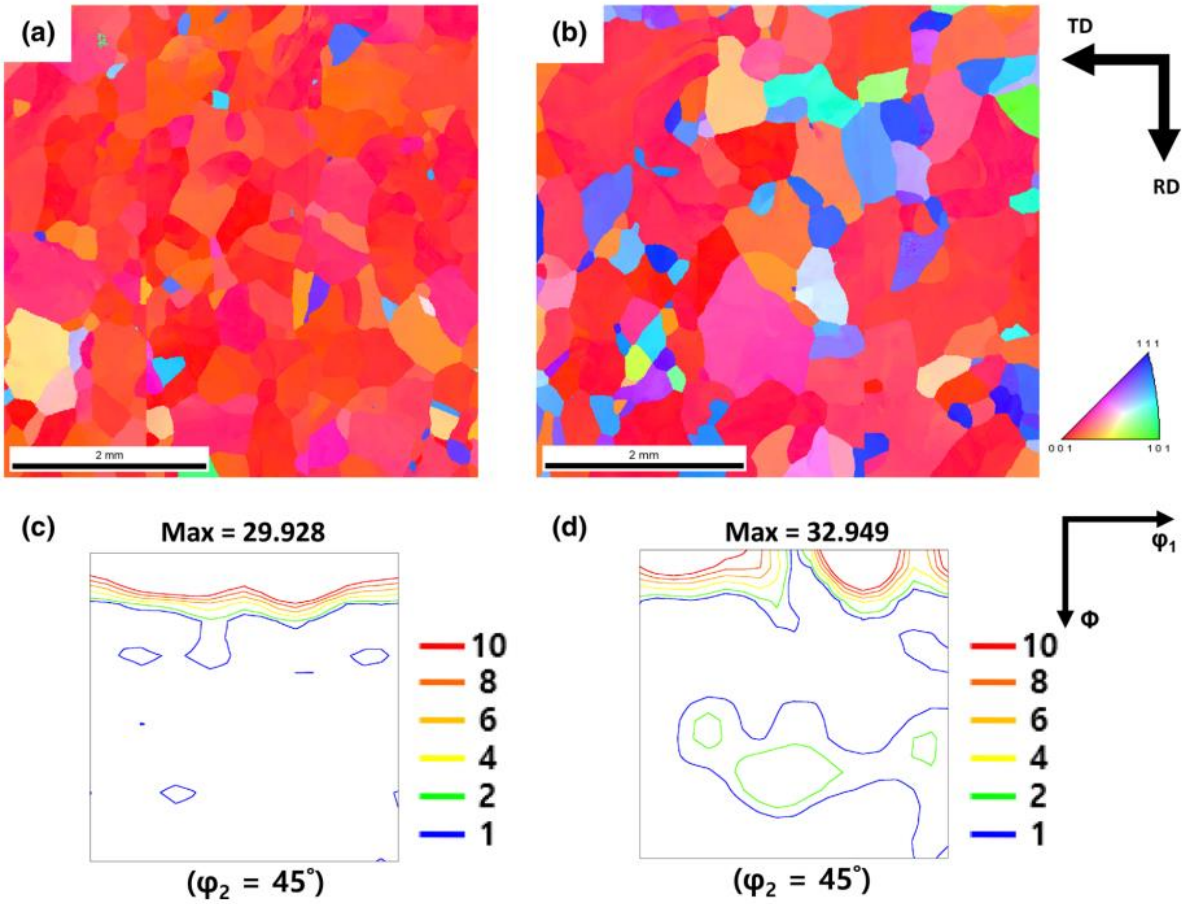

Figure 3.4. EBSD inverse pole figure ND maps of (a) position 1 and (b) position 19 of Fe-2wt%Si-1wt%Ni in Fig. 2.1b cooled at 16.7 ℃/min from 1000 to 900 ℃. (c) and (d) are ODFs at $\varphi_2 = 45^\circ$ section, respectively, for (a) and (b).

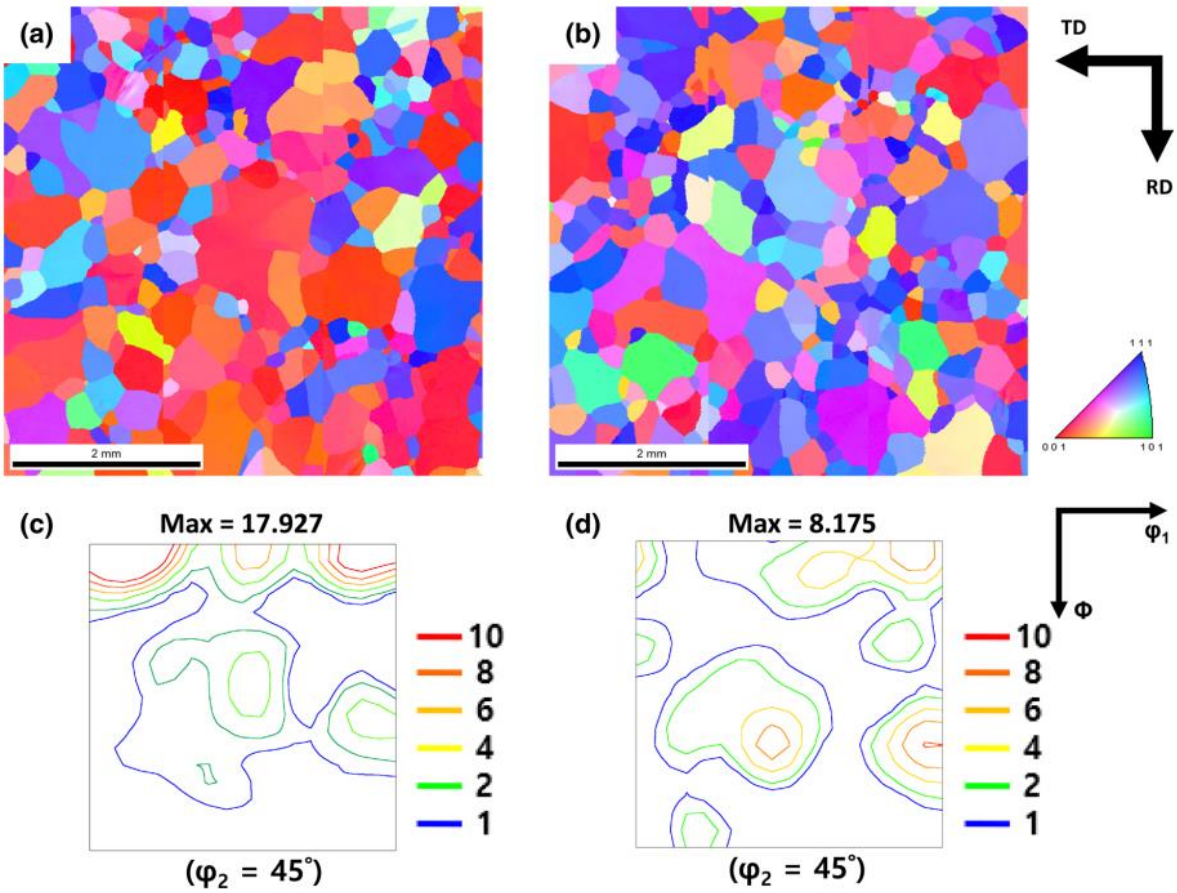

Figure 3.5. EBSD inverse pole figure ND maps of (a) position 1 and (b) position 19 of Fe-2wt%Si-1wt%Ni in Fig. 2.1b cooled at 0.1 ℃/min from 1000 to 900 ℃. (c)-(d) are ODFs at $\varphi_2 = 45^\circ$ section, respectively, for (a) and (b).

	5 min	1 h	3 h	6 h
{100} ± 15°, (%)				
Position 19	10.7	11.9	15.3	18.0
Position 13	9.4	13.2	16.2	13.3
Position 7	10.5	11.0	22.2	45.6
Position 1	8.9	17.0	27.5	66.0
{111} ± 15°, (%)				
Position 19	59.2	42.6	38.6	28.4
Position 13	61.7	45.3	37.0	30.6
Position 7	53.5	43.2	32.4	22.3
Position 1	55.5	37.6	27.8	7.3
Grain size, (μm)				
Position 19	109 (97)	154 (124)	212 (176)	246 (241)
Position 13	102 (89)	150 (142)	218 (208)	244 (250)
Position 7	114 (105)	175 (148)	236 (201)	279 (298)
Position 1	117 (102)	162 (159)	222 (249)	262 (299)

Table 3.1. Percentages of {100}<0vw> and {111}<uvw>, the average grain size of all grains and that of {100}<0vw> misorientation in parentheses for each position of Fe–2wt%Si–1wt%Ni heated for 5 min, 1 h, 3 h and 6 h at 1100 ℃. (See Fig. 3.1a for the heating cycle)

Position of analysis	{100}±15°, (%)	{111}±15°, (%)	Grain size, (μm)
Position 19	18.0	28.4	246 (241)
Position 13	13.3	30.6	244 (250)
Position 12	18.9	22.4	236 (239)
Position 11	23.7	31.7	238 (212)
Position 10	22.8	26.7	244 (228)
Position 9	27.4	29.4	253 (246)
Position 8	34.3	24.1	268 (266)
Position 7	45.6	22.3	279 (298)
Position 1	66.0	7.3	262 (299)

Table 3.2. Percentages of {100}<0vw> and {111}<uvw>, the average grain size of all grains and that of {100}<0vw> misorientation in parentheses for each position of Fe–2wt% Si–1wt%Ni heated for 6 h at 1100 ℃. (See Fig. 3.1a for the heating cycle)

Chapter 4. Evolution of {100}<0vw> texture induced by compressive stress in Fe-2wt%Si-1wt%Ni

4.1. Experimental procedure

An ingot of Fe-2wt%Si-1wt%Ni, which was manufactured by vacuum induction melting, was used as a starting material. The ingot was hot rolled to 2.3 mm and cold rolled to 0.35 mm thickness. Sheet specimens of 80 mm × 40 mm × 0.35 mm were prepared for heat treatment.

To check the effect of uniaxial compressive stress on the development of a cube-on-face {100}<0vw> texture, specimens were positioned in two different ways during heat treatment as shown in Fig. 4.1. One specimen was positioned in such a way that the broad 80 mm × 40 mm face lay horizontally to the nickel plate as shown in Fig. 4.1a, in which case the uniaxial stress on the center of the specimen is 13.3 Pa, being sufficiently small. The other specimen was positioned in such a way that the 80 mm × 40 mm face lay vertically to the nickel plate as shown in Fig. 4.1b, in which case the uniaxial stress on the center is 1519 Pa, being larger than that in Fig. 4.1a by almost 100 times. The stress on the Ni substrate is 26.6 Pa and 3038 Pa, respectively, in Fig. 4.1a and b. Since the

sample of 10 mm × 10 mm × 0.35 mm for EBSD measurements was taken out from the center of the specimen, the stress on the sample is 13.3 Pa and 1519 Pa, respectively, in Fig. 4.1a and b. The stress on the top is zero and increases to the maximum toward the bottom. The reason why the nickel plate is used to support the specimen is to minimize the effect of the shear stress between the specimen and the plate arising from the difference in the thermal expansion coefficient [20].

In order to find out the optimum holding time in the γ phase region needed for the development of the {100}<0vw> texture, each specimen was held for 1 min, 15 min and 60 min after being heated to 1120 ℃ of the γ phase region at 10 ℃/min. Then, the specimens were cooled to 970 ℃ for 120 min followed by being cooled to room temperature in the furnace. In our previous work on in-situ X-ray diffraction of Fe-2wt%Si-1wt%Ni [24], the (α + γ) two phase region started at ~900°C and the γ single phase region started at ~1000°C. Therefore, 1120°C and 970°C are expected to be, respectively, in the γ single phase region and the (α + γ) two phase region. We observed that recrystallization of Fe-2wt%Si-1wt%Ni steel occurred at ~700°C. The grain size after recrystallization was 17.5 μm, being similar regardless whether the specimens was placed horizontally (Fig. 4.1a or vertically (Fig. 4.1b)), but the high uniaxial stress (Fig. 4.1b) turned out to produce the grain size much larger than that of the low uniaxial stress (Fig. 4.1a) after α → γ → α phase transformation. Then, how can the

uniaxial stress increase the percentage of {100}<0vw> texture?

We could think of two possible causes for the increase of the grain size. One would be that the uniaxial stress increases the barrier for nucleation of α from γ during cooling due to the increase of the strain energy, which is proportional to the Young's modulus. Since {100}<0vw> grains on the surface have the lowest Young's modulus, their nucleation would be favored, increasing the cube-on-face texture. The other would be the recrystallization of α during heating, which would increase the γ grain size. In order to find out which of the two is the cause for the increase of the grain size, the specimens positioned in Fig. 4.1a and b were heated only to 700 ℃ of the α phase region at 10 ℃/min, held for 60 min, cooled to room temperature in furnace. In this heat treatment, only recrystallization would occur without the phase transformation between α and γ.

To study the effect of the percentages of {100}<0vw> on the magnetic properties, three specimens with different percentages of {100}<0vw> and {111}<uvw> were prepared. For measurements of magnetic flux density and core loss, specimens with the size of 60 mm × 60 mm × 0.35 mm were prepared. The first and second specimens were prepared by annealing at 1120 ℃ for 60 min with the 60 mm × 60 mm face, respectively, vertical (as shown in Fig. 4.1b) and horizontal (as shown in Fig. 4.1a) to the nickel plate. The third specimen was prepared under the same condition as the first specimen except that it was annealed at 970 ℃ for 60 min, which is

the (α + γ) two phase region. The magnetic flux density at 5000 A/m (B_{50}) and the core loss $W_{15/50}$, which was determined at a magnetic flux density of 1.5 T and 50 Hz, were measured by the MPG200D instrument (BrockHaus Measurements).

The texture evolution after the heat treatment was analyzed by electron back-scattered diffraction (EBSD, EDAX/Hikari) attached to a field emission scanning electron microscope (FESEM, SU5000, HITACHI). The EDAX/TSL software was used to analyze the orientation relationship. The specimen surface was polished in < 100 um thickness to the final stage of colloidal silica (OP-s, 0.04 μm).

4.2. Results and discussion

Fig. 4.2a and d shows, respectively, the inverse pole figure (IPF) normal direction (ND) map and the orientation distribution function (ODF) sectioned at φ_2 = 45° for the Fe-2wt%Si-1wt%Ni specimen heat treated with the broad face horizontal to the nickel plate at 1120 ℃ holding for 1 min, cooled to 970 ℃ for 120 min and cooled to room temperature in the furnace. Percentages of {100}<0vw> and {111}<uvw> were 11.1% and 62.6%, respectively, which were determined using the criteria of {100}<0vw> ± 15°. Fig. 4.2b and e shows, respectively, the IPF ND map and the ODF for the Fe-2wt%Si-1wt%Ni specimen heat treated at 1120 ℃ for 15 min with the other condition being the same as that of Fig. 4.2a. Percentages of {100}<0vw> and {111}<uvw> were 17.5% and 49.7%, respectively. Fig. 4.2c and f shows, respectively, the IPF ND map and the ODF for the Fe-2wt%Si-1wt%Ni specimen heat treated at 1120 ℃ for 60 min with the other condition being the same as that of Fig. 4.2a. Percentages of {100}<0vw> and {111}<uvw> were 30.9% and 37.0%, respectively. The average grain sizes of Fig. 4.2a, b and c were 144 μm, 156 μm and 170 μm, respectively, which was determined by converting the grain area into the diameter using an image analyzer software (EDAX/TSL software).

Fig. 4.3a and d shows, respectively, the IPF ND map and the ODF

for the Fe-2wt%Si-1wt%Ni specimen heat treated with the broad face vertical to the nickel plate at 1120 ℃ for 1 min, cooled to 970 ℃ for 120 min and cooled to room temperature in the furnace. Percentages of {100}<0vw> and {111}<uvw> were 65.9% and 16.5%, respectively. Fig. 4.3b and e shows, respectively, the IPF ND map and the ODF for the Fe-2wt%Si-1wt%Ni specimen heat treated at 1120 ℃ for 15 min with the other condition being the same as that of Fig. 4.3a. Percentages of {100}<0vw> and {111}<uvw> were 77.8% and 4.8%, respectively. Fig. 4.3c and f shows, respectively, the IPF ND map and the ODF for the Fe-2wt%Si-1wt%Ni specimen heat treated at 1120 ℃ for 60 min with the other condition being the same as that of Fig. 4.3a. Percentages of {100}<0vw> and {111}<uvw> were 81.1% and 2.1%, respectively. The average grain sizes of Fig. 4.3a, b and c were 168 μm, 196 μm and 237 μm, respectively. Fig. 4.4a, where the average grain size of α is plotted against the holding time, shows how horizontal and vertical positions of the specimens affect the grain size.

Figs. 4.2 and 4.3 show that entirely different textures were developed according to the specimen position. The percentage of {100}<0vw> was 11.1% in Fig. 4.2a but it increased abruptly to 65.9% in Fig. 4.3a. The percentage of {100}<0vw> texture in Fig. 4.2 was increased from 11.1% to 17.5% and 30.9% with increasing holding time from 1 min to 15 min and 60 min, respectively, but the dominant texture was still γ fiber. In Fig. 4.3, however, the percentage of {100}<0vw> was increased from 65.9% to 77.8% and 81.1% with

increasing holding time from 1 min to 15 min and 60 min, respectively. The percentage of {100}<0vw> in both Figs. 4.2 and 4.3 has increasing tendency with holding time but the major texture was different between Figs. 4.2 and 4.3. This aspect is shown in Fig. 4.4b, where the percentages of {100}<0vw> and {111}<uvw> are plotted against holding time.

Our previous research [20] showed the development of a strong cube-on-face texture when a slight tension was applied by self-load during heat treatment. A strong {100}<0vw> texture was developed in Fe-1wt%Si by heat treatment for 5 min at 1100 ℃. However, a strong γ fiber texture was developed when the specimen composition was changed to Fe-2wt%Si-1wt%Ni under the same condition. This different behavior between Fe-1wt%Si and Fe-2wt%Si-1wt%Ni was attributed to the grain size difference. If the grain size of γ is relatively small in the γ phase region, the number of four grain corners with a very low nucleation barrier is relatively large. Since the nucleation of the α grain with {100}<0vw> is favored only on the surface, the large number of four grain corners, which would increase the number of nuclei inside the bulk compared to that on the surface, would provide the unfavorable condition for the development of the {100}<0vw> texture. If the grain size of γ is relatively large, however, the development of the {100}<0vw> texture is favored. This aspect was supported by the previous experiment that the strong {111}<uvw> texture was changed to the strong {100}<0vw> texture when the holding time

was increased from 5 min to 24 h, resulting in the pronounced increase of the grain size [20].

Comparing the stress between horizontal and vertical positions, the compressive stress applied to the cross-sectional area of the specimen center is 13.3 Pa in Fig. 4.1a whereas it is 1519 Pa in Fig. 4.1b. Figs. 4.2 and 4.3 show that the high compressive uniaxial stress is responsible for the development of the strong {100}<0vw> texture. The strong {100}<0vw> texture in Fig. 4.3 cannot be explained by the large grain size because the γ nuclei would be under the tensile stress during α → γ transformation because γ has a lower molar volume than α and therefore the compressive uniaxial stress would decrease the nucleation barrier and increase the number of nuclei, thereby decreasing the grain size. Therefore, the larger grain size in Fig. 4.3 than in Fig. 4.2 would result from γ → α transformation during cooling rather than from α → γ transformation during heating. During cooling, the compressive uniaxial stress would increase the nucleation barrier and decrease the number of nuclei, thereby increasing the grain size.

One possible cause for the effect of the high uniaxial stress on the strong {100}<0vw> texture in Fig. 4.3 would be to increase the barrier for nucleation of α from γ during cooling due to the increase of the strain energy, which is proportional to the Young's modulus. As mentioned before, {100}<0vw> grains on the surface have the lowest Young's modulus and thereby their nucleation would be

favored, increasing the cube-on-face texture.

There is another possible effect of the compressive stress. This would be that the compressive stress may induce recovery or recrystallization in such a way to increase the grain size. To confirm this possibility, the two specimens, one of which has the position of Fig. 4.1a and the other of which has the position of Fig. 4.1b, were heated to the recrystallization temperature of 700 ℃ and held for 60 min, then cooled to room temperature in the furnace.

Fig. 4.5a and c shows, respectively, the IPF ND map and the ODF of the Fe-2wt%Si-1wt%Ni specimen heat treated at 700 ℃ with the position of Fig. 4.1a. Percentages of {100}<0vw> and {111}<uvw> were 6.5% and 61.0%, respectively. Fig. 4.5b and d shows the IPF ND map and the ODF of the Fe-2wt%Si-1wt%Ni specimen heat treated at 700 ℃ with the position of Fig. 4.1b. Percentages of {100}<0vw> and {111}<uvw> were 9.7% and 57.1%, respectively. The average grain sizes of Fig. 4.5a and b were 17.5 μm and 18.4 μm, respectively. The texture and the grain size in Fig. 4.5a and b are not much different, indicating that the large grain size in Fig. 4.3 does not come from recovery or recrystallization but come from the phase transformation.

However, if only the grain size is considered, Fig. 4.2c with the grain size of 170 μm should have a higher percentage of {100}<0vw> than Fig. 4.3a with the grain size of 168 μm. Therefore, a much higher percentage of 65.9% {100}<0vw> in Fig. 4.3a than

30.9% {100}<0vw> in Fig. 4.2c cannot be explained by the grain size alone. This means that the high compressive stress has an additional effect. One possibility we can think of is that the inhibition effect of the compressive stress on nucleation is larger in the bulk than on the surface. As a result, the surface nucleation of {100}<0vw> becomes dominant.

Based on understanding of the texture development, we could prepare the specimens with different percentages of {100}<0vw> in the Fe-2wt%Si-1wt%Ni alloy. Then, we studied how the {100}<0vw> texture could affect the magnetic properties such as magnetic flux density and iron loss. For this, three Fe-2wt%Si-1wt%Ni specimens of 60 mm × 60 mm × 0.35 mm with different percentages of {100}<0vw> were manufactured as shown in Fig. 4.6. Fig. 4.6a and d shows, respectively, the IPF ND map and the ODF for the Fe-2wt%Si-1wt%Ni specimen heat treated with the position of Fig. 4.1b at 1120 ℃ holding for 60 min, cooled to room temperature in the furnace. Percentages of {100}<0vw> and {111}<uvw> were 78.4% and 3.2%, respectively. Fig. 4.6b and e shows, respectively, the IPF ND map and the ODF for the Fe-2wt%Si-1wt%Ni specimen heat treated with the position of Fig. 4.1a with the other condition being the same as that of Fig. 4.6a. Percentages of {100}<0vw> and {111}<uvw> were 35.6% and 26.9%, respectively. Fig. 4.6c and f shows, respectively, the IPF ND map and the ODF for the Fe-2wt%Si-1wt%Ni specimen heat treated at 970 ℃ for 60 min, cooled to room temperature in the furnace.

Percentages of {100}<0vw> and {111}<uvw> were 0.7% and 81.3%, respectively. The average grain sizes of Fig. 4.6a, b and c were 235 μm, 170 μm and 127 μm, respectively.

Table 4.1 shows the magnetic properties of the Fe-2wt%Si-1wt%Ni specimens with different percentages of {100}<0vw> and {111}<uvw>. Fig. 4.6a, which has the maximum percentage, 78.4%, of {100}<0vw> and the minimum percentage, 3.2%, of {111}<uvw>, produces the highest magnetic flux density of B_{50} = 1.75 and the lowest iron loss of $W_{15/50}$ = 2.19. Fig. 4.6b, which has 35.6% of {100}<0vw> and 26.9% of {111}<uvw>, produces B_{50} = 1.69 and $W_{15/50}$ = 2.34. Fig. 4.6c, which has the minimum percentage, 0.7%, of {100}<0vw> and the maximum percentage, 81.3%, of {111}<uvw>, produces B_{50} = 1.61 and $W_{15/50}$ = 2.50. These results show that the magnetic properties strongly depend on the percentage of {100}<0vw>.

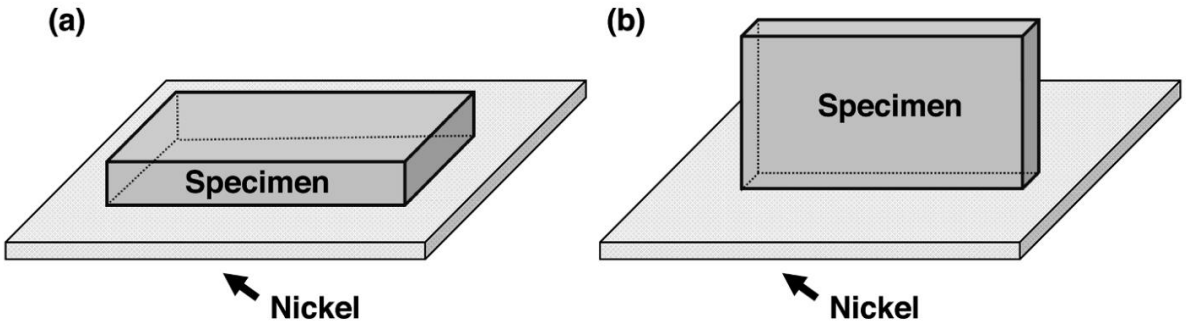

Figure 4.1. Schematics showing how specimens were placed during heat treatment. The 80 mm × 40 mm face of the specimens lay (a) horizontally and (b) vertically to the nickel plate.

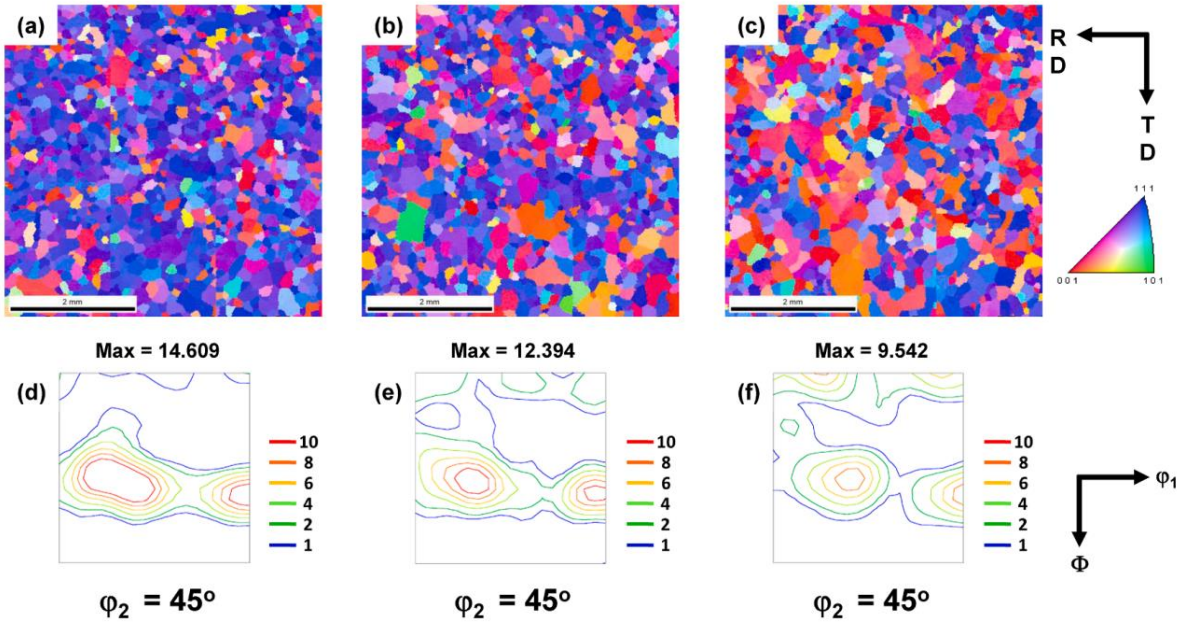

Figure 4.2. EBSD inverse pole figure ND maps of Fe-2wt%Si-1wt%Ni specimens with the 80 mm × 40 mm face lying horizontally to the nickel plate, which were held at 1120 ℃ in H_2 for (a) 1 min, (b) 15 min, and (c) 60 min. (d), (e) and (f) are ODFs at φ_2 = 45° section for (a), (b) and (c), respectively.

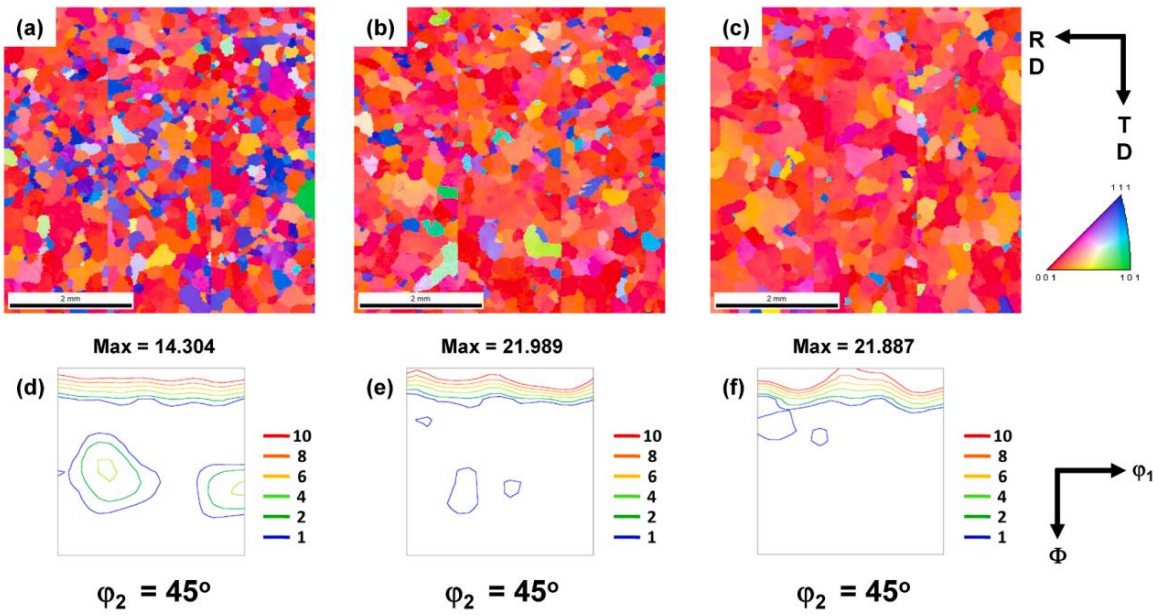

Figure 4.3. EBSD inverse pole figure ND maps of Fe-2wt%Si-1wt%Ni specimens with the 80 mm × 40 mm face lying vertically to the nickel plate, which were held at 1120 ℃ in H_2 for (a) 1 min, (b) 15 min, and (c) 60 min. (d), (e) and (f) are ODFs at φ_2 = 45° section for (a), (b) and (c), respectively.

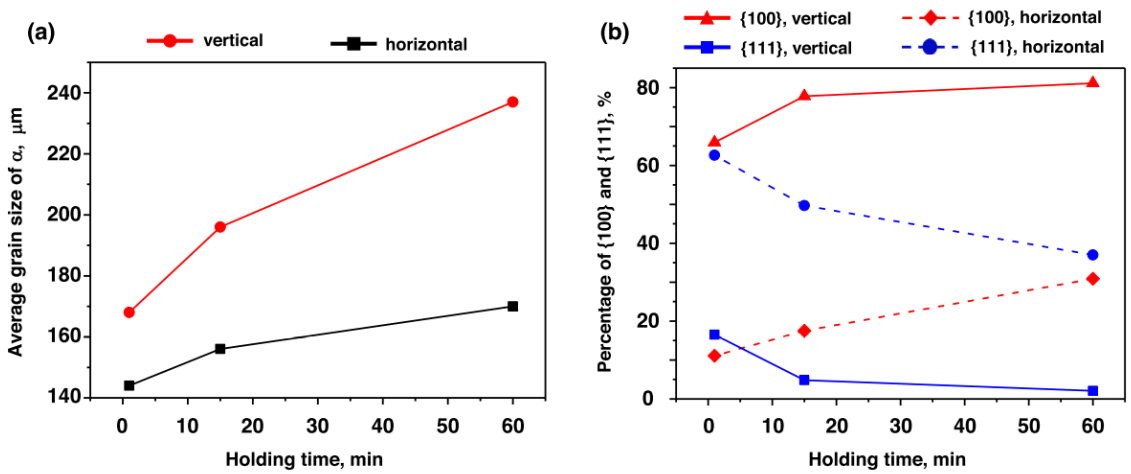

Figure 4.4. (a) The average grain size of α varying with the holding time at 1120 ℃ for the specimens with the 80 mm × 40 mm face lying vertically (red circle) and horizontally (black square) to the nickel plate. (b) Percentages of {100} (red triangle and rhombus) and {111} (blue circle and square) varying with annealing time. Solid and dashed lines represent the specimens with the 80 mm × 40 mm face, respectively, lying vertically and horizontally to the nickel plate.

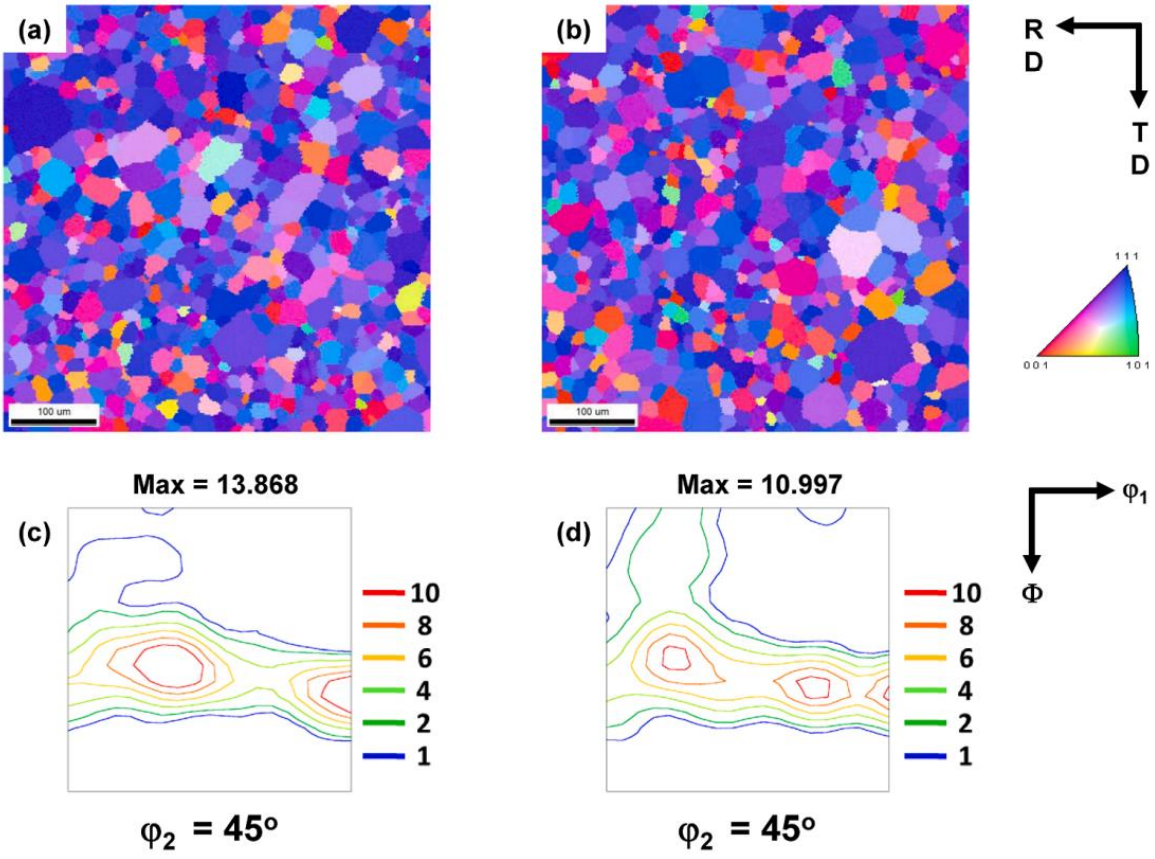

Figure 4.5. EBSD inverse pole figure ND maps of Fe-2wt%Si-1wt%Ni specimens annealed at 700 ℃ for 60 min in H_2 with the 80 mm × 40 mm face lying (a) horizontally and (b) vertically to the nickel plate. (c) and (d) are ODFs at φ_2 = 45° section for (a) and (b), respectively.

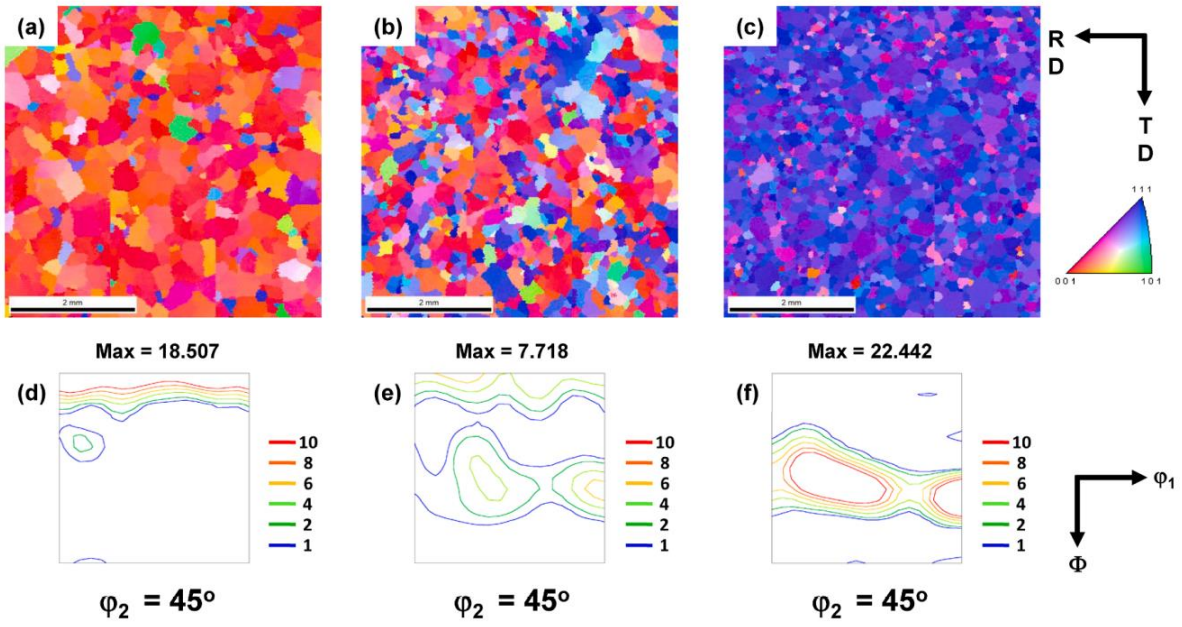

Figure 4.6. EBSD inverse pole figure ND maps of Fe-2wt%Si-1wt%Ni specimens for measurement of magnetic properties. (a) 78.4%, (b) 35.6% and (c) 0.7% of {100}. (d), (e) and (f) are ODFs at φ_2 = 45° section for (a), (b) and (c), respectively.

	{100}±15°	{111}±15°	B_{50}	$W_{15/50}$
Fig. 4.6a	78.4%	3.2%	1.75	2.19
Fig. 4.6b	35.6%	26.9%	1.69	2.34
Fig. 4.6c	0.7%	81.3%	1.61	2.50

Table 4.1. Magnetic properties of Fe-2wt%Si-1wt%Ni alloys with a different texture.

Chapter 5. Conclusions

- The evolution of the {100}<0vw> texture was favored by the small tensile stress, non-oxidizing atmosphere, large grain size and the high cooling rate in the two phase (α + γ) region. The Fe-2wt%Si-1wt%Ni specimen prepared under the small tensile stress and flowing H_2 at 1000 sccm at the cooling rate of 16.7 ℃/min with the grain size increased by 6 h heat treatment at 1100 ℃ produced the {100}<0vw> texture as high as 92.6%

- A compressive stress imposed on the specimen, depending how the specimen is positioned during heat treatment, was shown to affect the evolution of the cube-on-face texture in Fe-2wt%Si-1wt%Ni. The specimen positioned with the broad face vertical to the specimen holder has the larger percentage of {100}<0vw> than that with the broad face horizontal to the specimen holder. Based on this result, specimens with a different percentage of {100}<0vw> could be manufactured. The Fe-2wt%Si-1wt%Ni specimen with 78.4% of {100} and 3.2% of {111} had excellent magnetic properties of B_{50} = 1.75 and $W_{15/50}$ = 2.19. However, specimen with 0.7% of {100} and 81.3% of {111} had relatively poor magnetic properties of B_{50} = 1.61 and $W_{15/50}$ = 2.50.

.

Bibliography

[1] A.J. Moses, Scripta Materialia 67 (2012) 560-565.

[2] H.-K. Park, J.-H. Kang, C.-S. Park, C.-H. Han, N.-M. Hwang, Materials Science and Engineering: A 528 (2011) 3228-3231.

[3] H.-S. Shim, T.-W. Na, J.-S. Chung, S.-B. Kwon, K. Gil, J.-T. Park, N.-M. Hwang, Scripta Materialia 116 (2016) 71-75.

[4] T.-Y. Kim, H.-S. Shim, S. Kim, S. Choi, T.-W. Na, D. Kwon, N.-M. Hwang, Materials Characterization 156 (2019) 109845.

[5] T.-Y. Kim, T.-W. Na, H.-S. Shim, Y.-K. Ahn, Y.-K. Jeong, H.N. Han, N.-M. Hwang, Metals and Materials International 27 (2021) 5114-5120.

[6] T.-W. Na, H.-K. Park, C.-S. Park, H.-D. Joo, J.-T. Park, H.N. Han, N.-M. Hwang, Metals and Materials International 24 (2018) 1369-1375.

[7] T.-Y. Kim, H.-K. Kim, Y.-K. Jeong, Y.-K. Ahn, H.-S. Shim, D. Kwon, N.-M. Hwang, Metals and Materials International 26 (2020) 1200-1206.

[8] H.-S. Shim, N.-M. Hwang, Korean J. Met. Mater. 52 (2014) 663-687.

[9] K. Günther, G. Abbruzzese, S. Fortunati, G. Ligi, steel research international 76 (2005) 413-421.

[10] L. Zhang, P. Yang, J. Wang, W. Mao, Journal of Materials Science 51 (2016) 8087-8097.

[11] M. Mehdi, Y. He, E.J. Hilinski, L.A. Kestens, A. Edrisy, Acta Materialia 185 (2020) 540-554.
[12] R. Liang, P. Yang, W. Mao, Journal of Magnetism and Magnetic Materials 457 (2018) 38-45.
[13] M. Sanjari, Y. He, E.J. Hilinski, S. Yue, L.A. Kestens, Scripta Materialia 124 (2016) 179-183.
[14] M. Gallaugher, A. Samimi, T.W. Krause, L.C. Clapham, R.R. Chromik, Metallurgical and Materials Transactions A 46 (2015) 1262-1276.
[15] L. Xie, P. Yang, D. Xia, W. Mao, Journal of Magnetism and Magnetic Materials 374 (2015) 655-662.
[16] M. Mehdi, Y. He, E.J. Hilinski, A. Edrisy, Texture Evolution of a 2.8 wt% Si Non-Oriented Electrical Steel during Hot Band Annealing, IOP Conference Series: Materials Science and Engineering, vol 375, IOP Publishing, 2018, p. 012014.
[17] T. Tomida, Journal of applied physics 79 (1996) 5443-5445.
[18] J.K. Sung, D.N. Lee, D.H. Wang, Y.M. Koo, ISIJ international 51 (2011) 284-290.
[19] S.-B. Kwon, Y.-K. Ahn, Y.-K. Jeong, T.-Y. Kim, J.-T. Park, H.N. Han, N.-M. Hwang, Materials Characterization 165 (2020) 110380.
[20] Y.-K. Ahn, S.-B. Kwon, Y.-K. Jeong, J.-U. Cho, T.-Y. Kim, N.-M. Hwang, Materials Characterization 170 (2020) 110724.
[21] D.N. Lee, Scripta Metallurgica et Materialia 32 (1995) 1689-1694.

[22] J.W. Cahn, Acta metallurgica 4 (1956) 449-459.
[23] I.-R. Sohn, J.-S. Kim, S. Sridhar, ISIJ International 55 (2015) 2008-2017.
[24] Y.-K. Ahn, Y.-K. Jeong, T.-Y. Kim, J.-U. Cho, N.-M. Hwang, Materials Today Communications 25 (2020) 101307.
[25] N. Hwang, D.Y. Yoon, Journal of materials science 32 (1997) 4847-4855.

요약(국문 초록)

전기강판 재료에서 감마 → 알파 상변태를 이용한 표면핵생성 및 {100} 집합조직 형성 연구

전기강판 재료는 크게 방향성 전기강판과 무방향성 전기강판으로 분류된다. 방향성 전기강판의 경우 일반적으로 변압기용 소재로 쓰이며 한 방향으로 배향돼 있는 {110}<001>, Goss 집합조직을 사용한다. Goss 집합조직은 한 방향으로 자기적 특성이 우수하다. 반면 무방향성 전기강판의 경우 대표적으로 전기자동차 모터 혹은 발전기용 소재에 사용되는데 이때 가장 이상적인 집합조직은 {100}<0vw>, cube-on-face 집합조직이다. Cube-on-face 집합조직은 회전 방향으로 자기적 특성이 균일하면서 우수하다. Cube-on-face 집합조직은 ND 방향으로 <100>, 동시에 ND와 수직인 방향으로는 랜덤하게 배향돼 있다.

연구가 활발히 진행돼 있고 상용화된 Goss 집합조직과는 달리 cube-on-face 집합조직은 연구가 부족한 실정이다. Cube-on-face 집합조직은 꿈의 재료로 알려져 있다.

본 연구는 “감마 → 알파 상변태 열처리시 시편에 응력을 가하게 되면 핵생성장벽이 낮은 {100} 핵이 표면에 유도되고 더불어 벌크 내부보다 표면에 핵생성이 우세하다면 {100}<0vw> 집합조직 형성”에 대한 가설을 제시한다. 인장응력 혹은 압축응력을 가하여 cube-on-face 집합조직 형성의 핵심인 표면핵생성 연구를 하였다.

주요어 : 전기강판; 상변태; 큐브 온 페이스; {100}; 집합조직; EBSD
학번 : 2017-28846